CHARACTERIZATION OF WEAR AND DYNAMIC PERFORMANCE OF INTERSTAGE SEALS FOR ELECTRIC SUBMERSIBLE PUMPS

A Thesis

by

ROBERT BYRD HURE

Submitted to the Office of Graduate and Professional Studies of
Texas A&M University
in partial fulfillment of the requirements for the degree of

MASTER OF SCIENCE

Chair of Committee,	Adolfo Delgado
Committee Members,	Luis San Andrés
	Chao Ma
Head of Department,	Andreas A. Polycarpou

May 2019

Major Subject: Mechanical Engineering

ABSTRACT

Electric Submersible Pumps (ESPs) increase head of process fluid in oil production from within the well. An ESP comprises of a pump, seal, and motor section oriented vertically. The pump section includes multiple centrifugal pump stages guided radially by interstage seals. ESP mechanical failure most commonly results from severe vibrations in the pump section that increase in magnitude as interstage seal clearances increase. Interstage seals wear from the gas, liquid, and abrasives pumped through them.

This project studies wear, dynamic performance, and leakage of interstage seals for ESPs using a component-level test rig. Silicon carbide, tungsten carbide, and reinforced thermoplastic seals with and without axial grooves are tested. Tests evaluate the impact of different gas concentrations, clearances, and sand concentrations under water lubrication. Results show axial grooves do not significantly impact wear rate, but do significantly increase leakage. Increasing gas volume fraction modestly increases wear rate and induces low frequency vibration orbit variability. Carbide seals have superior wear resistance compared to that of reinforced thermoplastic seals. Radial clearance and sand concentration does not significantly impact wear rate for carbide seals in the range of tested sand concentrations, suggesting sliding wear is the dominant mechanism. Results suggest plain carbide seals should be used in ESPs. Future work should focus on protecting carbide seals from fracture failure, which remains a concern for the integrity of seals.

ACKNOWLEDGEMENTS

There are so many people that have helped me during my time at Texas A&M and on my path to graduate school. First and foremost, I would like to thank my advisor Dr. Adolfo Delgado for giving me this opportunity and providing support and sound technical advice. I would also like to thank Dr. Abhay Patil for his frequent advice and humor, which preserved my sanity and will. Bryant Myers provided valuable assistance during data collection.

The support of Hector Casillas and Shell was fundamental. The groundwork for this project was laid by Dr. Gerald Morrison and numerous students that came before me, including Changrui Bai, Andrew Johnson, Nicolas Carvajal, Ramy Saleh, Dhezhi Zheng, Daniel Steck, Burak Ayilldiz, and Wenjie Yin. I'd also like to thank all the students in Dr. Delgado's research group that provided good company and camaraderie throughout my studies.

I would not have been able to pursue my Master's degree without the love and support of my parents, Mike and Elizabeth, as well as my fiancée Brenna. I also owe a debt of gratitude to all the educators that have taken an interest in my learning throughout my extended education, particularly Dr. Jennifer Steele and Dr. Peter Kelly-Zion.

CONTRIBUTORS AND FUNDING SOURCES

This work was supported by a thesis committee consisting of Professor Adolfo Delgado and Professor Luis San Andrés of the Department of Mechanical Engineering and Professor Chao Ma of the Department of Manufacturing and Mechanical Engineering Technology. Additional support was provided by Dr. Abhay Patil of the Texas A&M Turbomachinery Laboratory.

Graduate students Burak Ayyildiz and Wenjie Yin of the Texas A&M Turbomachinery Laboratory collected approximately 70% of "reinforced thermoplastic I" data. Undergraduate student Bryant Myers of the Texas A&M Turbomachinery Laboratory assisted the collection of data related to "reinforced thermoplastic II" and carbide tests with an initial radial clearance of 127 um. The student completed all other work.

Shell Oil Company provided financial support.

NOMENCLATURE

C/R	Clearance to radius ratio
PV	Equivalent pressure multiplied by tangential rotor velocity
L/D	Ratio of length to diameter
ESP	Electric Submersible Pump
GVF	Gas Volume Fraction
OEM	Original Equipment Manufacturer
PEEK	Polyetheretherketone thermoplastic
PFA	Perfluoroalkoxy thermoplastic
PTW	Potassium Titanate Whiskers
SCFR	Short Carbon Fiber Reinforcement
SiC	Silicon Carbide
VFD	Variable Frequency Drive
WC	Tungsten Carbide

TABLE OF CONTENTS

Page

LIST OF FIGURES

Page

LIST OF TABLES

Page

1. INTRODUCTION

Electric Submersible Pumps (ESPs) are widely used in the oil industry to generate artificial lift that maintains or boosts oil well production. The majority of oil wells require artificial lift, while roughly 20% of oil wells utilize ESPs [1]. An ESP comprises of a pump, seal, and motor section oriented vertically. The pump section includes multiple centrifugal stages guided radially by interstage seals[1]. The process fluid passing through the pump is often a mixture of gas, liquid, and sand[2] in deep subsea applications. Sand may originate from hydraulic fracturing of the well or from the well itself. At different stages during the lifetime of the well, the process fluid may be primarily water or primarily oil [2].

ESPs are considered a commodity equipment in the oil industry [1], but because of their location down well are expensive to replace in deep subsea applications [3]. Replacing an ESP may cost as much as forty times the actual cost of the ESP in deep subsea wells [4]. As the use of ESPs in deep subsea application increases, greater attention has focused on ESP reliability. Pump reliability is the quality of consistently providing the expected flow and head requirements to the fluid. Increases in reliability manifest in longer operating lifetimes, which decrease significantly in environments with high amounts of sand or gas [5]. Oil companies aim to achieve ESP lifetimes of seven years, while an OEM in 2012 projected two year lifetimes [6].

---

[1]Interstage seal is the common nomenclature used in the turbomachinery industry. A seal limits flow through a secondary flow path and has a pressure differential across it, which is true of the component of interest. The oil and gas industry has traditionally called this a journal bearing. A journal bearing primarily provides direct support for the rotor, which is also true of the component of interest. The component may also be referred to as a bushing, which is a plain hollow cylinder around a rotating shaft.

[2] Also known as three-phase flow (solid, liquid, gas).

Statistics compiled by Durham et al. [7] found excessive pump vibration from unbalance as the primary cause of ESP mechanical failure. Previous work at the Texas A&M Turbomachinery Laboratory show pump vibrations increase in amplitude over the lifetime of the pump as clearances within the interstage seals increase and impeller erosion creates greater rotor unbalance [4]. Interstage seal clearances increase primarily from abrasive wear among the seal, shaft, and sand particles. Limiting seal wear rate could slow the growth of vibrations, potentially increasing the lifetime of the ESP.

This work focuses on evaluating the impact of different materials on the wear rate of plain and axially grooved seals. While seals do not typically have axial grooves, axial grooves could reduce wear by allowing free sand particles to pass through the grooves without being crushed between the shaft and seal at the expense of increased leakage and reduced pump performance.

2. LITERATURE REVIEW

This section provides background information on interstage seals and ESPs. The basic rotordynamics of ESPs and seals is discussed, followed by a discussion on wear mechanics, previous experiments on ESPs, and interstage seal material properties.

As stated previously, statistics compiled by Durham et al. [7] found excessive pump vibration from rotor unbalance as the primary cause of ESP mechanical failure. Interstage seals typically provide the majority of rotor support and are important to the rotordynamics of ESPs. Interstage seals support the rotor mainly by generating direct stiffness through the Lomakin effect [8], which results from the pressure differential across the seal. The presence of gas greatly affects direct stiffness and damping coefficients generated by an interstage seal. Iwatsubo and Nishino [9] studied force coefficients in a plain annular seal, finding coefficients decrease continuously as gas volume fraction (GVF) increases.

Modeling by Childs et al. [3] of ESP data from Forsberg [10] found increased clearances in the impeller labyrinth seals and interstage seals decreases all stiffness and damping coefficients provided by the seals, resulting in more severe vibrations. Initial radial clearances in interstage seals are typically between 75 and 150 μm for 45 mm diameter shafts, producing clearance to radius ratios (C/R) around 0.004. Tighter installation clearances are avoided due to the possibility of fracture failure during pump installation or shaft concentricity tolerances that would prevent assembly.

Seal clearances increase from material removal resulting from sliding wear, three-body abrasion, and erosion. Sliding wear occurs when shaft and seal roughness peaks contact due to inadequate fluid film thickness. Greater loads and slower speeds generally produce thinner fluid

films [11]. For full hydrodynamic lubrication to prevent sliding wear, the fluid film must be at least ten times greater than the surface roughness of the seal and shaft [11]. Polishing decreases surface roughness, decreasing the coefficient of friction and the film thickness required to prevent sliding wear. Sliding wear is governed by the *PV* value[3], coefficient of friction, and material abrasive resistance [12]. Severe sliding wear can result in heat checking, producing cracks or fracture. Heat checking occurs when two loaded bodies in sliding contact experience a high coefficient of friction, creating high local temperatures. Thermomechanical stress from the load, Coulomb friction, and thermal stress can initiate fracture [13].

Free particles within the fluid, called third bodies, can accelerate material removal through three-body abrasion. If the diameter of the third body exceeds the thickness of the fluid film, the free particle is crushed and removes material from the shaft and seal. Xuan et al. [14] found three-body abrasive wear for small particle sizes is minimized when the shaft and seal are significantly harder than the abrasive particles. Abrasive resistance also increases with material hardness [15]. Figure 2-1 lists hardness values of some common materials, reprinted from [16]. With large clearances, erosion from free particles incident on the seal and shaft can create wear.

[3] *PV* is the product of equivalent pressure and tangential rotor velocity. Equivalent pressure is the load divided by the seal length and diameter.

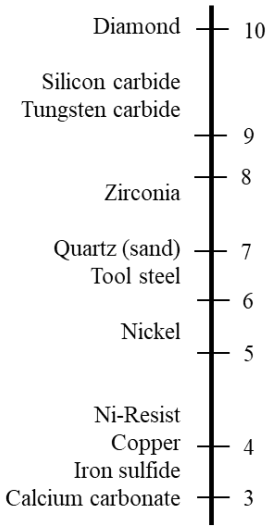

Figure 2- 1 Material hardness values on Mohs scale. Reprinted from [16].

Morrison's research group at the Texas A&M Turbomachinery Laboratory investigated dynamic performance and wear of different ESPs under various operating conditons. Morrison's students built a test rig to study a three stage mixed flow[4] ESP manufactured for test purposes with tungsten carbide interstage seals and shaft sleeves [17]. Carvajal [17], Saleh [18], and Zheng [19] investigated the reliability of the pump with a mixture of sand, air, and water to simulate process fluid. Tests utilized 100 mesh sand with a mean diameter of 187 μm and interstage seals with an initial radial clearance of 150 μm. Results show pump impellers eroded over the duration of the test, increasing the rotor unbalance and overall pump vibrations. Interstage seal clearances increased during the test from wear, which coincided with increased pump vibrations. Interstage seal wear rate increased when inlet gas volume fraction increased from 0% to 15%.

[4]Centrifugal ESP pumps are either mixed flow or radial flow. Radial flow impellers discharge fluid radially, while mixed flow impellers discharge fluids radially and axially. Mixed flow impellers are common on higher flow applications.

Inspection of the tungsten carbide seals and sleeves revealed polishing, circumferential grooves, and small axial cracks from heat checking. Bai [20] attributes the grooves to three-body abrasion created by sand rotating in the seal. Greater wear occurred at the outlet than the inlet of the seals. Morrison et al. [4] suggest sand created abrasive grooves at the inlet that crushed sand into smaller, sharper particles that polished and wore the outlet of the seal.

Steck [21] performed tests on a different ESP using the experimental setup developed by Carvajal, finding interstage seal wear rate increased in the presence of gas. Chen [22] found interstage seal clearances and shaft vibrations increased over the duration of testing on a four-stage ESP. Inspection of the interstage seals and shaft sleeves also revealed circumferential grooves.

In order to focus on interstage seals, Bai [20] and Johnson [23] developed a component-level test rig that simulates operating conditions for an interstage seal in an ESP. Bai performed experiments that varied rotor unbalance, GVF, and operating speed in order to evaluate their impact on rotordynamics in the component-level test rig lubricated with water and air. Seals operated with a 3.45 bar pressure differential at a speed of 3600 RPM. Bai found vibration orbit variability increases with GVF, and smaller clearances produce smaller vibration orbits.

The present study utilizes the component-level rig developed by Bai and Johnson to evaluate the impact of different materials and geometries on wear and dynamic performance. Tests include three types of materials: self-mated tungsten carbide and silicon carbide, and reinforced thermoplastic seals paired with stainless steel shaft sleeves. Tungsten carbide is chosen as a baseline because it is commonly used for interstage seals in ESPs. Silicon carbide is chosen for its potential to resist abrasion and heat checking better than tungsten carbide. Reinforced thermoplastic is chosen for its fracture resistance.

Silicon carbide (SiC) is hard, strong, and inert, making it a good candidate for tribology applications [24]. Silicon carbide also has a low coefficient of thermal expansion, preventing thermal growth and thermal stresses that can lead to failure at high operating temperatures [25]. The main drawback of silicon carbide is its brittle nature, which leads to fracture failure [24].

Andersson [26] studied SiC paired with each other or hardened 440 stainless steel using a pin-on-disk setup in water. Andersson found SiC paired with SiC exhibits a coefficient of friction of 0.3 that fell to roughly 0.03 after roughly 400 meters of contact regardless of load. Andersson also found polishing of the lubricated SiC corresponds to a decrease in coefficient of friction and wear rate.

Tungsten carbide (WC) is similar to silicon carbide, but has a significantly higher density and strength than SiC despite having a comparable hardness value. WC has a lower specific heat than SiC, causing heat generation from rubbing to create higher local temperatures and larger thermal expansions that produce heat checking. The properties of tungsten carbide vary based on the substance and concentration used to bind tungsten carbide particles together [27]. Table 2-1 shows a comparison between SiC and WC, adapted from [24] [27] [29]. Wakigawa et al. [28] studied vertical pumps used to drain water from rivers and oceans, finding SiC slightly outperformed WC. Hardness and wear resistance had a strong positive correlation.

Table 2- 1 Carbide material properties. Adapted from [24] [27] [29].

Property	**Silicon carbide** [24]	**Tungsten carbide** [27] [29]
Density (g/cm3)	3.17	14.9
Modulus of Elasticity (GPa)	430	614
Poisson's ratio (-)	0.13	0.21
Hardness (GPa)	31	30
Fracture Toughness (MPa-$m^{1/2}$)	3.2	3
Compressive Strength (GPa)	2.5	4.3
Specific Heat (J/g-K)	0.95	0.2
Thermal Conductivity (W/m-K)	110	84
Thermal Expansion (1/K)	4.1×10^{-6}	3.3×10^{-6}

Unlike tungsten carbide and silicon carbide, reinforced thermoplastics are lightweight and flexible, making fracture failure unlikely [30]. Carbon fibers are commonly used to reinforce thermoplastics because of the high specific tensile strength, high modulus of elasticity, and wear resistance [31]. Material properties of reinforced thermoplastics vary significantly based on the thermoplastic, fiber, fiber structure, and fiber surface treatment. A common thermoplastic used in tribology is polyetheretherketone (PEEK), which is used in the present study. Yamamoto and Takashima [32] observed a high wear rate for neat (unreinforced) PEEK in water. Clarke and Allen [33] show reinforcing PEEK increases the material hardness, creating a material more resistant to wear. Hanchi et al. [34] show higher temperatures degrade material properties in reinforced thermoplastics.

Xie et al. [35] studied PEEK reinforced by carbon fibers or potassium titanate whiskers (PTW) using pin-on-disk experiments in tap water. Reinforced PEEK exhibited a coefficient of friction of roughly 0.01 and wear less than one fiber layer thickness. Coefficient of friction decreased during a wear-in period, settling to a steady state value. Neat PEEK had significantly higher wear rates and coefficients of friction. Swierczek [36] replaced a bronze bushing with a

reinforced PEEK bushing in a water pump, which increased the bushing lifetime from 2 years to 5 years due to the abrasive resistance of the reinforced PEEK.

This study considers axial grooves on the seal as an alternate geometry. Axial grooves could reduce wear in an ESP by allowing free sand particles to pass through the grooves without being crushed between the shaft and seal to create three-body abrasion. The amount of sand that enters axial grooves instead of the thin film region will depend on seal clearances.

3. EXPERIMENTAL FACILITIES

Figure 3-1 shows the test rig developed by Bai [20] and Johnson [23], featuring one air loop and two water loops. An auger driven by a stepper motor adds sand to the main water flow loop before the slurry passes through the main diaphragm pump and nutating disk flow meter. The test rig utilizes diaphragm pumps to minimize wear on the sand as it circulates through the test loop. Diaphragm accumulator tanks attached to each pump outlet decrease pressure and flow fluctuations caused by the positive displacement pumps.

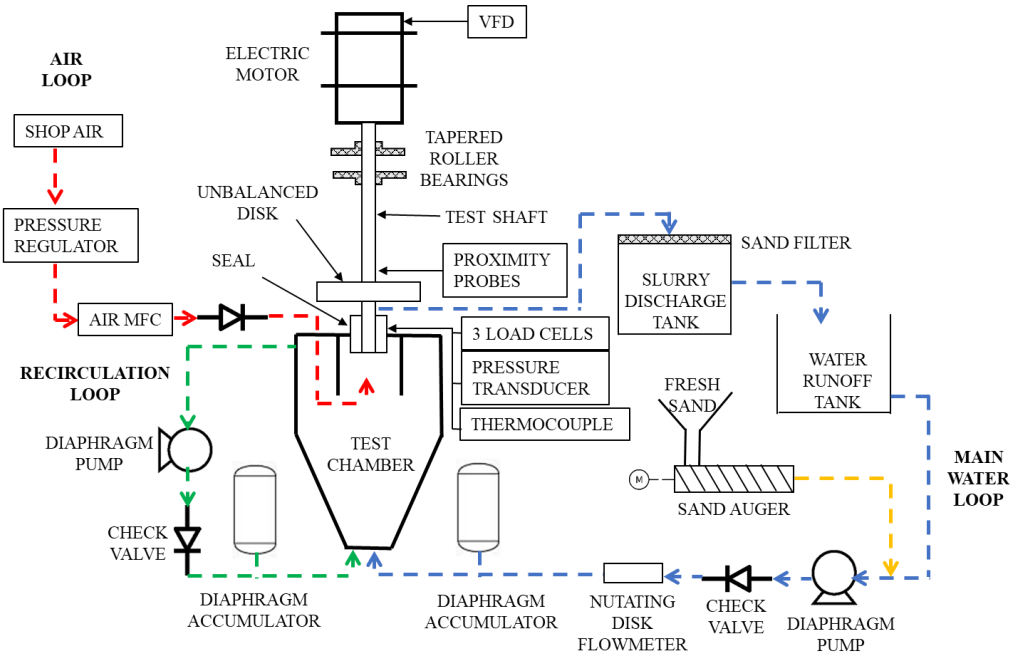

Figure 3- 1 Schematic diagram of the test rig. Two water loops and one air loop provide controlled quantities of sand, water, and air to the seal inlet.

The main diaphragm pump forces water and sand to flow vertically into the test chamber or through the recirculation loop. The recirculation pump collects sand and water from the test chamber and discharges to the chamber inlet. The recirculation loop keeps sand suspended by

increasing slurry velocity inside the test chamber. The conical bottom of the test chamber forces settling sand back into the upward flow stream from the incoming slurry. A mass flow controller measures and regulates air supplied by the facility compressor. Air is introduced in the upper half of a cylinder below the seal to ensure it passes through the seal.

After passing through the seal, the slurry discharges into the sand collection tank. A particulate filter removes sand from the flow loop, and air vents to the atmosphere. Water from the top of the sand collection tank feeds into the runoff tank and re-enters the main water flow loop. Allowing sand to pass through the seal only once allows proper control of particulate size, as sand could be crushed passing through the seal. Discharge from the test chamber is directly above the seal and vents to atmosphere; assuming atmospheric pressure above the seal allows chamber gauge pressure to serve as the differential pressure across the seal.

The test chamber moves on a pair of linear bearings that allow assembly and disassembly periodically during testing for measurement and inspection of the seal and shaft sleeve. Dowel pins between the test chamber and discharge box ensure the test chamber and seal will not rotate or change alignment during disassembly and re-assembly. At axial planes located 25% and 75% of the seal length, multiple micrometer measurements are taken to find the minimum and maximum diameter within each axial plane. These four measurements are recorded and summed to calculate rotor and stator diameters, then subtracted to produce clearance. Individual micrometer measurements have a precision of ±12 μm diametrically, producing an uncertainty of ±2 μm for each average radius and ±4 μm for radial clearance.

Figure 3-2 shows a model of the test rotor. A flexible rubber tire coupling connects the test shaft to the motor driven by a variable frequency driver (VFD). Two self-aligning rolling element bearings provide radial support to the shaft. A 304 stainless steel disk with screws

inserted to create 0.483 g-m of rotor unbalance simulates an ESP impeller. Above the unbalanced disk, two orthogonal proximity probes measure the shaft vibration orbit. The test sleeve secures to the end of the shaft below the unbalanced disk. Sleeves are manufactured to produce a 150 μm radial clearance between the shaft and sleeve.

Table 3-1 summarizes variables kept constant during testing to simulate operating conditions in an ESP. The chosen sand concentration of 0.057 g/L water would be considered moderate-heavy in an ESP [16]; however, the relationship between sand concentration at the inlet of an ESP and sand concentration passing through interstage seals has not been established. Sieve analysis of the sand reveals a mean diameter of 196 μm and a median diameter of 187 μm [4]. The water flowmeter has an uncertainty of ±1.5%, or ±0.3 LPM for a typical 20 LPM flowrate. The air flowmeter has an uncertainty of ±1.5 LPM. For an equal mixture of gas and liquid by volume, this produces a value of 0.50 ±0.06 assuming typical flowrates of 20 LPM. The sand auger produces a sand concentration uncertainty of ±6% based on verification tests.

PV values are not presented because seals are unloaded. Dynamic forces could be calculated from load cell measurements or predicted using XLTRC2 to produce *PV* values. Shaft sleeve diameters vary slightly, producing tangential speeds of 8.1 or 9.0 m/s.

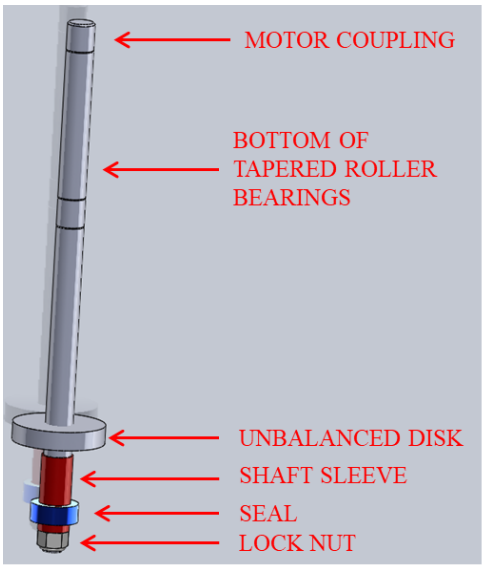

Figure 3- 2 Model of the test rotor. The shaft sleeve secures to the test rotor below the unbalanced disk using a lock nut. Proximity probes measure shaft vibration orbit above the unbalanced disk. Two roller bearings support the shaft near the top of the rotor, which couples to the electric motor

Table 3- 1 Experimental control variables

Variable description	Value	Unit
Differential pressure across seal	345	kPa
Sand concentration	0.057	g/L water
Shaft speed	3600	rpm
Rotor unbalance	0.483	g-m
Mean sand diameter	187	µm

4. TEST SEALS AND SHAFT SLEEVES

Figure 4-1 shows the silicon carbide seal and shaft sleeve tested with and without an 8 μm diamond coating. Tungsten carbide sleeves and seals without grooves are tested with geometries identical to the silicon carbide parts. Two axial grooves at opposite sides of the seal provide a path for sand particles passing through the carbide seal. Testing on seals without grooves provides a baseline to evaluate the impact of the grooves on wear rate and dynamic performance. Radial grooves on the top of the seal serve no purpose during testing; seals are installed with the radial grooves at the outlet of the seal. Nominal radial clearance between the carbide seal and sleeve are initially 15 or 127 μm. Tight initial radial clearances are chosen to investigate the impact on wear.

Two types of reinforced thermoplastic seals are tested with hardened stainless steel 440 sleeves. Reinforced thermoplastic I is a carbon-fiber reinforced perfluoroalkoxy (PFA), and reinforced thermoplastic II is a carbon-fiber reinforced PEEK. Figure 4-2 shows images of the reinforced thermoplastic seals and stainless steel shaft sleeves. Reinforced thermoplastics are tested with and without axial grooves. Both reinforced thermoplastics have initial radial clearances of roughly 127 μm. However, the reinforced thermoplastics absorb water, causing initial radial clearances to decrease when seals are wet and constrained from growing outward. Reinforced thermoplastic I requires thirty minutes to fully absorb water and produce an initial wet radial clearance of 89 μm, while reinforced thermoplastic II requires only ten minutes and creates an initial wet radial clearance of 112 μm. This produces growth rates of 1.3 μm/min for reinforced thermoplastic I and 3.0 μm/min for reinforced thermoplastic II. Tables 4-1 and 4-2 list seal dimensions and material properties, respectively.

Figure 4- 1 Silicon carbide seal and shaft sleeve

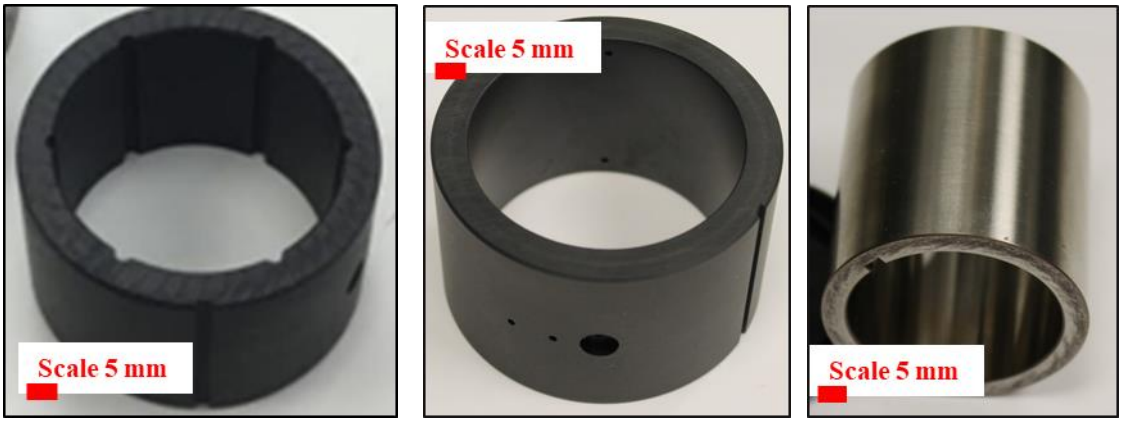

a) I with grooves b) II without grooves c) Test Sleeve

Figure 4- 2 Reinforced thermoplastics and test sleeve

Table 4- 1 Seal dimensions

Dimension	Reinforced thermoplastics	Carbides
Inner Diameter (mm)	47.8	43.0
Outer Diameter (mm)	61.2	65.0
Initial wet radial clearance (µm)	~100	15 or 127
Height (mm)	38.1	25.0

Table 4- 2 Reinforced thermoplastic and sleeve material properties provided by manufacturers

Property	**Seal I**	**Seal II**	**Hardened SS 440 shaft sleeve**
Density (g/cm3)	1.93	1.42	7.8
Tensile Strength (MPa)	99.3	130.3	1034
Tensile Modulus (GPa)	17.3		200
Flexural Strength (MPa)	14.5	172	
Flexural Modulus (GPa)	2.6	8.96	
Compressive Strength (MPa)	65.6	172	
Compressive Modulus (GPa)	24	3.7	
Thermal Expansion (1/K)	8.6×10^{-6}	45×10^{-6}	10.2×10^{-6}
Hardness (Shore D)	80	88	97 Rockwell
Melting Point (^{o}C)	260	340	

5. MODELING AND SIMULATIONS

XLTRC2 simulations are performed as a companion to experimental tests to provide insight into observed wear rates. Unless otherwise stated, simulations utilize conditions identical to experimental tests.

Seal geometries and test conditions are modeled using the programs Hseal_mix[5] and XLHsealH[6]. Seals without axial grooves are studied based on program capabilities. Seal and shaft material properties do not affect these predictions, as only geometry and test conditions contribute to seal reaction forces. Results and discussion of seal simulations are available in the Appendix.

Seal force coefficients are combined with a model of the test rotor to determine the impact of radial clearance on displacement and support forces using synchronous, steady state analysis. A more rigorous transient analysis was performed by Bai [20] on geometries identical to the reinforced seal using a fluid-structure interaction program to investigate subsynchronous vibrations. This simulation uses seal force coefficients at zero eccentricity regardless of shaft position, which is generally valid assuming the shaft reaches a quasi-steady state during orbital motion for eccentricities less than 0.8, according to seal simulations available in the Appendix.

Figure 5-1 shows the XLTRC2 predictions of the first two natural frequencies and associated damping ratios. XLTRC2 does not predict any other natural frequency below 2.5X operating speed. The first two natural frequencies had nearly identical mode shapes and significant damping ratios, which vary negligibly with clearance for both carbide and

[5] Copyright 2017 by Texas A&M University Turbomachinery Laboratory. All rights reserved. Dr. Luis San Andrés and Xueliang Lu

[6] Copyright 2010 by Texas A&M University. All rights reserved. Dr. Luis San Andrés

thermoplastic seals. Both are forward modes. Figure 5-2 shows the mode shape with 76 µm radial clearance.

Figures 5-3 & 5-4 show support forces and deflections change similarly for both seals as clearance varies. The force supplied by the roller bearings increases significantly as clearance increases, but the force supplied by the seal remains constant at roughly 60 N.

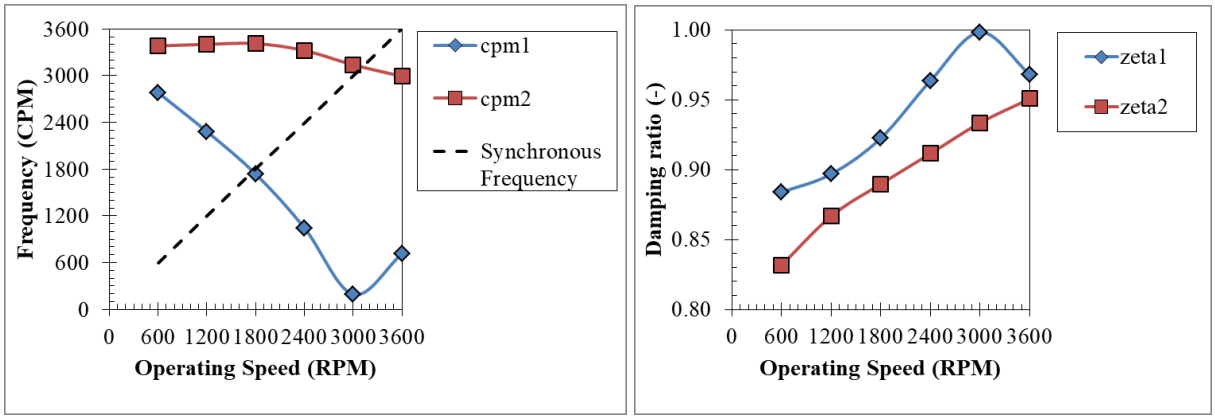

Figure 5- 1 Predicted damped natural frequencies and damping ratios for the reinforced thermoplastic seal with 127 µm radial clearance

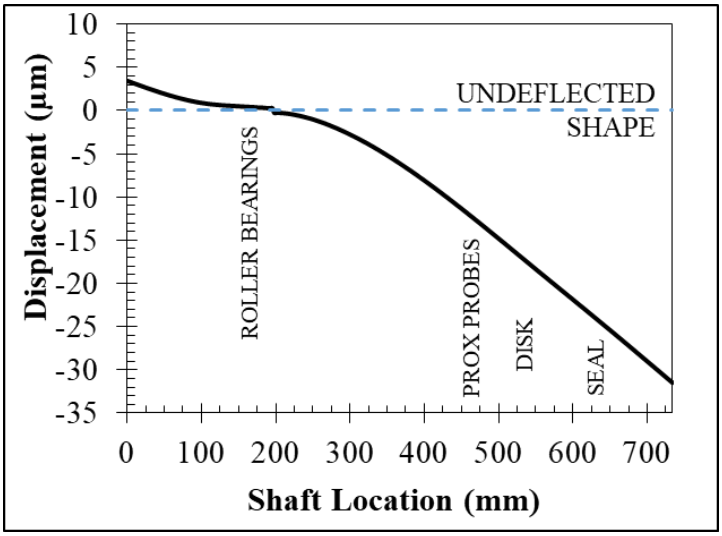

Figure 5- 2 Typical shaft vibrational mode. Roller bearings located around shaft location of 150 mm, and seal located near shaft location of 650 mm. Shown: reinforced thermoplastic seal, 76 µm radial clearance

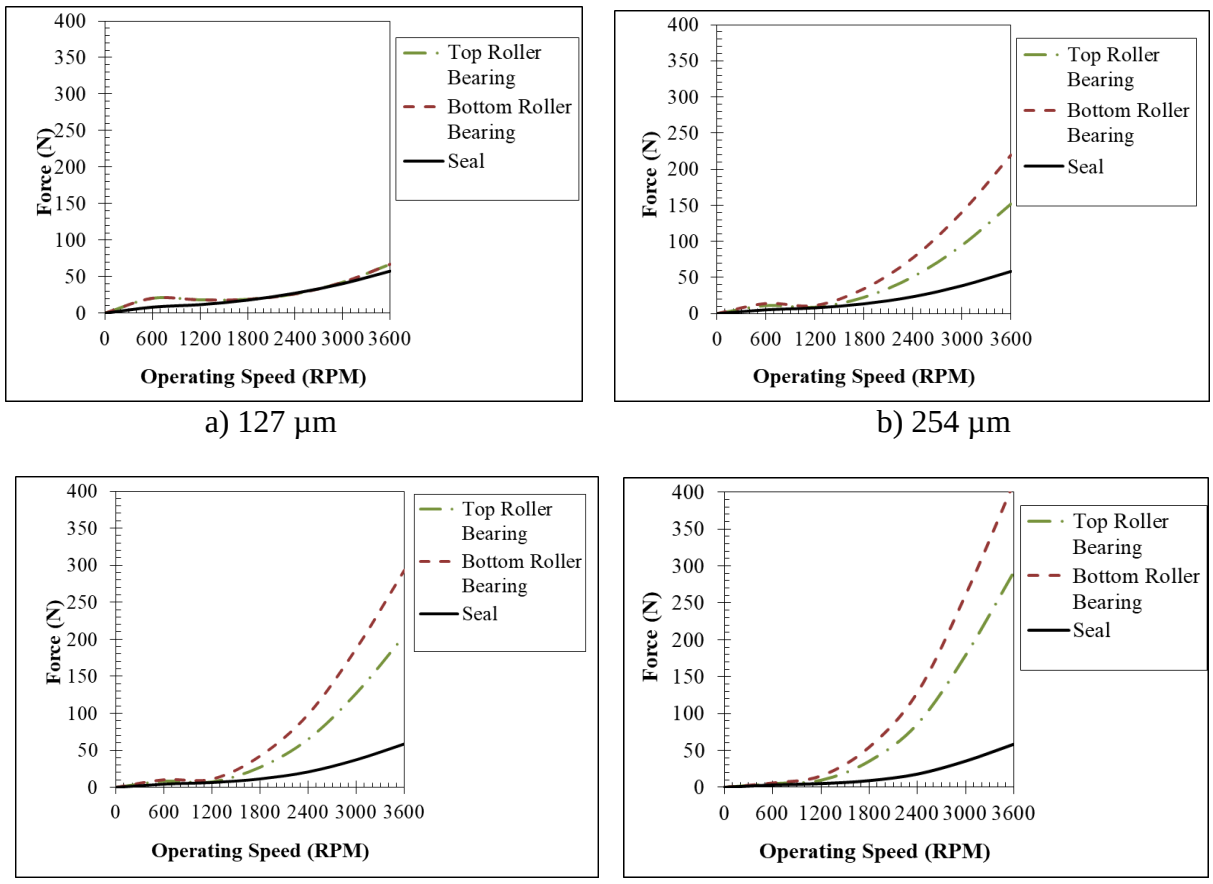

a) 127 µm b) 254 µm

c) 356 µm d) 508 µm

Figure 5- 3 Simulated support forces for different radial clearances in the reinforced thermoplastic seal at 0% GVF using a zero eccentricity approximation

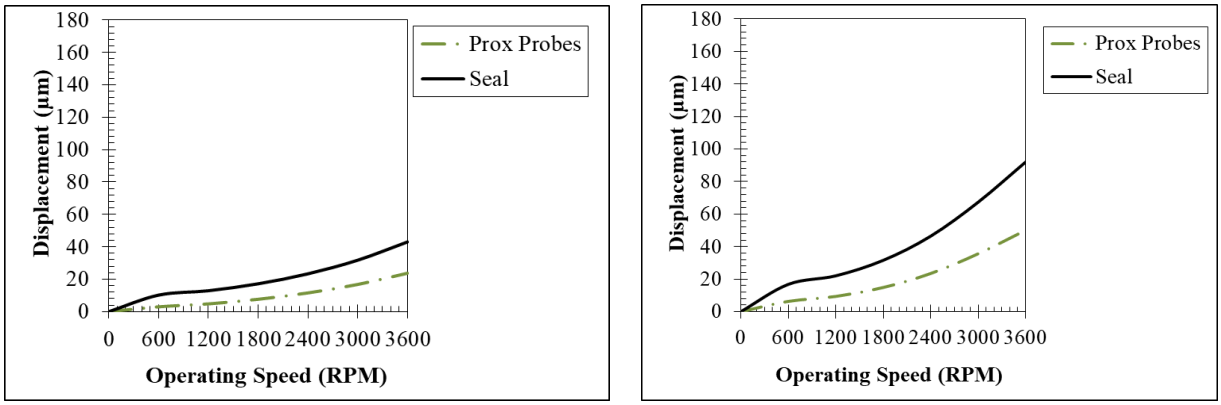

a) 127 µm b) 254 µm

c) 356 µm d) 508 µm

Figure 5- 4 Simulated peak displacement for different radial clearances in the reinforced thermoplastic seal at 0% GVF using a zero eccentricity approximation

Simulated displacement increases as clearance increases. Figures 5-5 & 5-6 show plots of minimum film thickness at different radial clearances for both seals. Minimum film thickness is equal to the difference between radial clearance and displacement. Mean sand diameter does not vary with clearance. Radial clearance is projected onto the vertical axis to illustrate its relation to sand particle size and minimum clearance.

Minimum film thickness is consistently greater than 30% of clearance for clearances above 150 µm, allowing the zero eccentricity approximation to hold in this range. For clearances less than sand diameters, sand is unable to enter the clearance and create three-body abrasion,

making sliding wear the predicted dominant mechanism. For minimum film thicknesses greater than sand diameters, the shaft does not deflect enough to crush the sand and create three-body abrasion, making slurry erosion the predicted dominant mechanism. For clearances greater than sand diameters and minimum film thicknesses less than sand diameters, sand is crushed between the shaft and seal to produce three-body abrasion. Greater shaft displacement is predicted for higher GVFs, extending the range of clearances that produce three-body abrasion. Figure 5-7 illustrates sliding wear, three-body abrasion, and slurry erosion. Simulations indicate changes in clearances will result in changes in wear mechanisms.

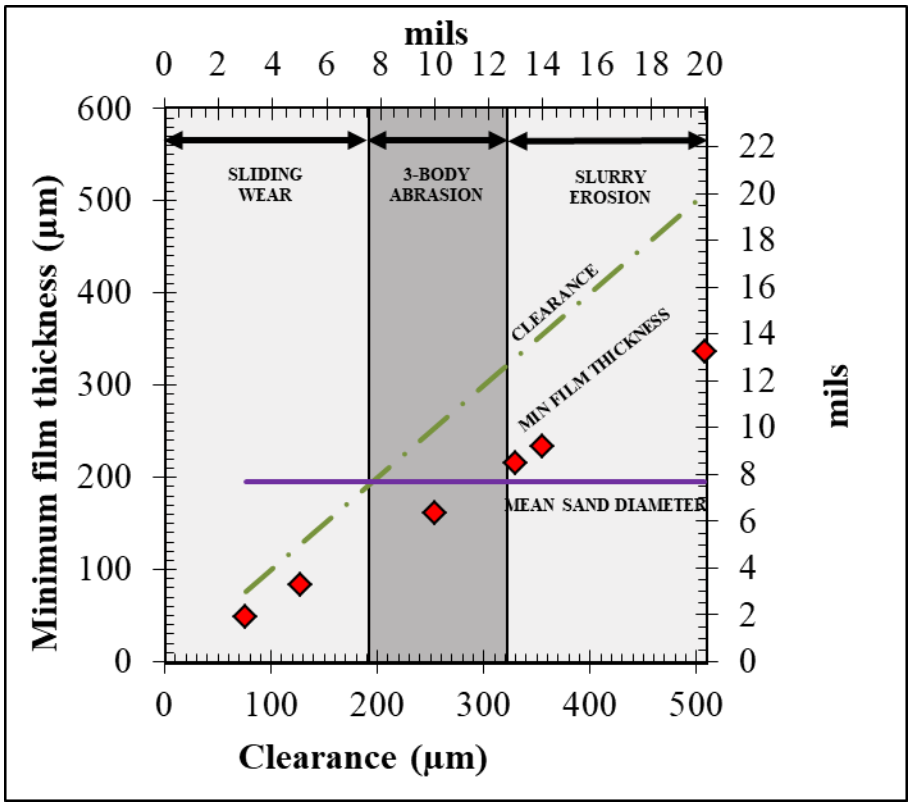

Figure 5- 5 Minimum film thickness for the reinforced thermoplastic seal using a zero eccentricity approximation at 0% GVF

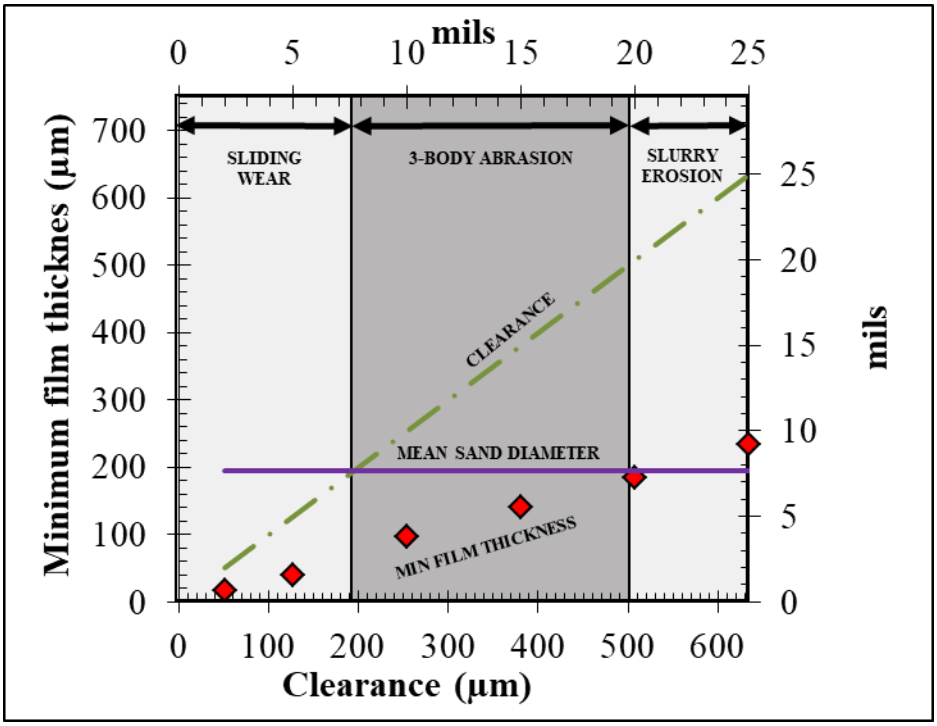

Figure 5- 6 Minimum film thickness comparison for the carbide seal using a zero eccentricity approximation at 0% GVF

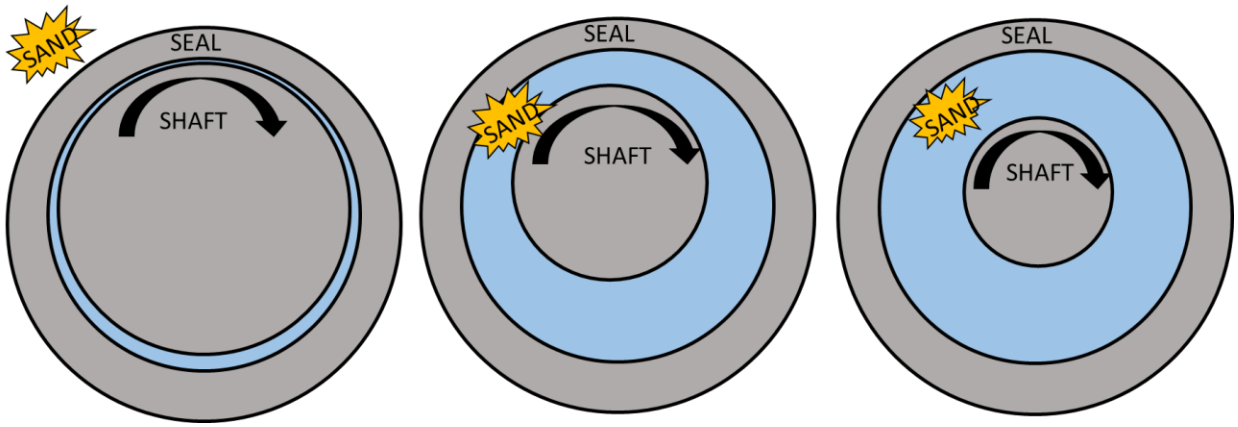

a) Sliding wear b) Three-body abrasion c) Slurry erosion

Figure 5- 7 Wear mechanism diagrams

6. EXPERIMENTAL RESULTS AND ANALYSIS

6.1 Silicon carbide tests with 15 µm initial radial clearance

Four tests are performed with grooved SiC seals having an initial radial clearance of 15 µm, as shown in Table 6-1. Test conditions are listed in the experimental facilities section. Test no. 3 ended prematurely when the shaft sleeve became loose due to a gasket failure. This problem was addressed and did not arise in other tests. Initial radial clearances are significantly smaller than any sand particles.

Figure 6-1 shows the clearance as a function of test hours. Clearances remain significantly smaller than sand particle sizes throughout testing. Wear rate, defined as the change in clearance with respect to time, decreases as testing progresses with the exception of test no. 4 when the GVF increased after 50 hours of testing to induce additional wear. Higher GVFs produce more wear. One test was performed on a seal and shaft sleeve with an 8 µm diamond coating. The diamond-coated set does not outperform the uncoated set at 80% GVF, although only 15 hours of data is available. Minimal wear on uncoated SiC left minimal room for improvement.

Figure 6-1 can be broken into wear of the seal and wear of the shaft sleeve, as shown in Fig. 6-2. Wear rate decreases on both the seal and sleeve as testing progresses. Wear concentrates on the shaft sleeve rather than the seal. According to Xuan et al. [14], equal wear is expected on the seal and sleeve when they are made of the same material with the same hardness. Xuan et al. tested components with minimal pressure differentials. A larger pressure differential may increase the axial velocity of the fluid and decrease the swirl ratio, causing the abrasive

particles to move with a greater velocity gradient between the shaft and particle than the velocity gradient between the seal and particle, creating greater shaft wear than seal wear.

Table 6- 1 SiC Test matrix with 15 µm initial radial clearance

No.	Coating	GVF (%)	Notes
1.	None	0	
2.	None	80	
3.	Diamond	80	Test ended after 15 hours due to installation error
4.	None	40 for 50 hours, 80 for 50 hours	

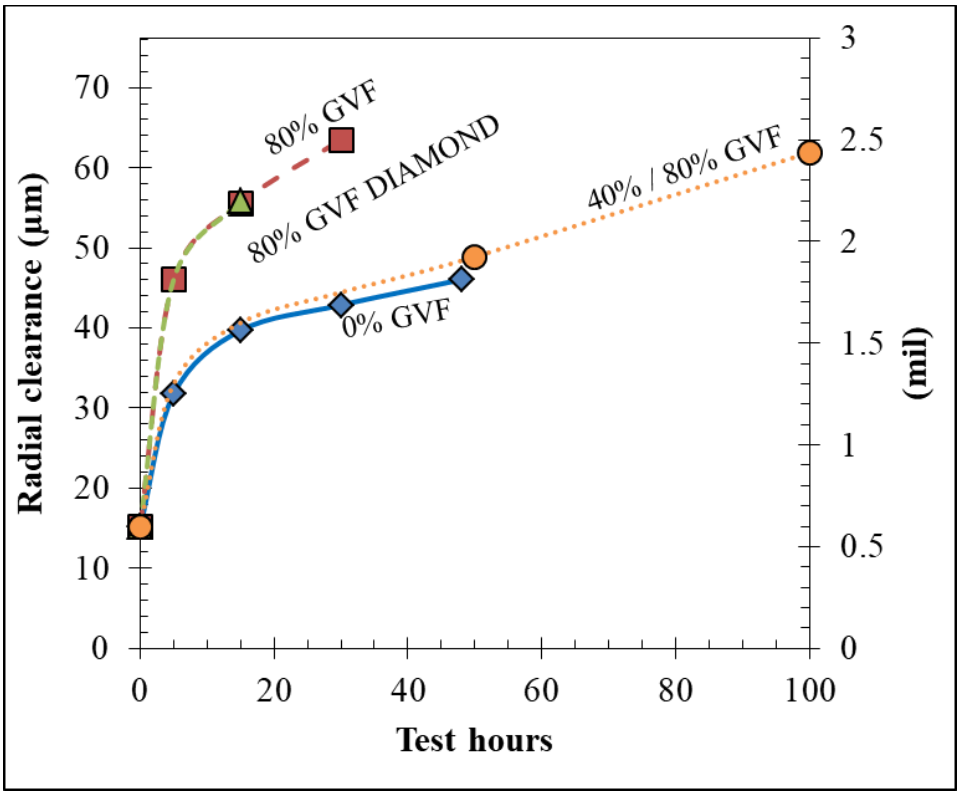

Figure 6- 1 Radial clearance as a function of test hours for SiC tests with an initial radial clearance of 15 µm

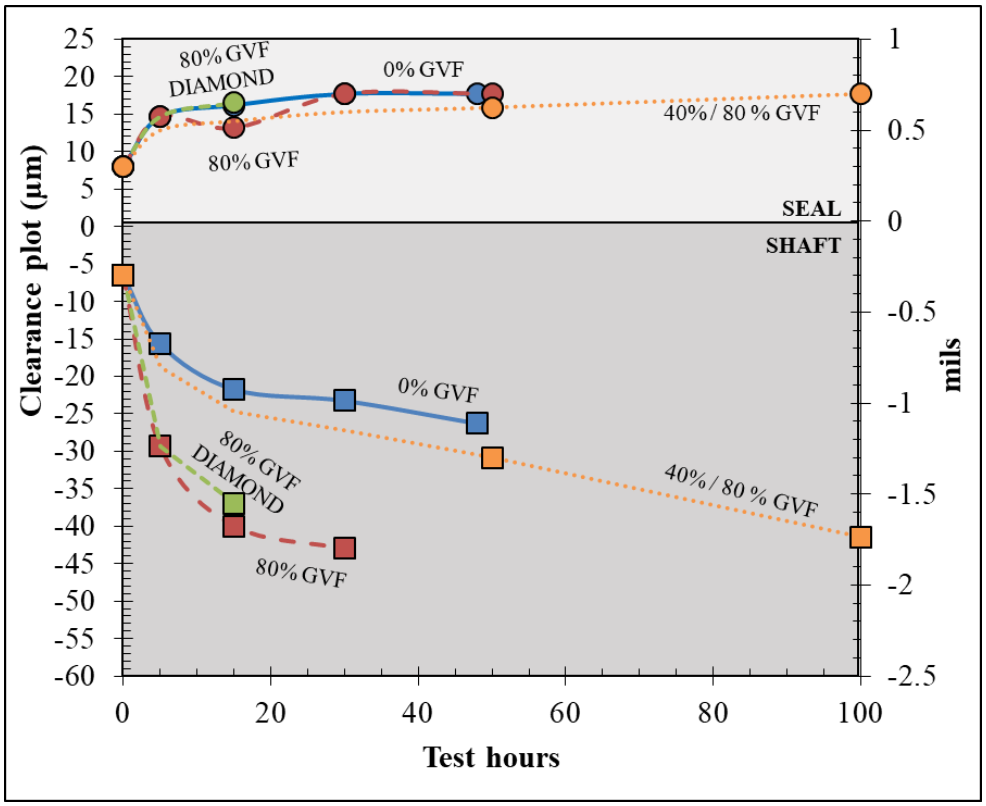

Figure 6- 2 Radial clearance as a function of seal and sleeve wear for SiC seals and shaft sleeves with an initial radial clearance of 15 µm

Figure 6-3 shows unbalanced disk shaft vibration orbits did not change significantly during testing, which is expected based on the minimal change in clearance. Vibration orbits shown at the unbalanced disk are larger than seal clearances despite the fact that simulations predicted larger displacements within the seal than at the unbalanced disk. The discrepancy in vibrational orbit diameter may result from the presence of a dead band clearance. Figures 6-4 & 6-5 show unbalanced disk vibrational orbits had a radius of roughly 50 µm at 600 rpm, which increases only slightly as speed increases. The dead band clearance likely results from loose roller bearings, which would move radially before receiving support from the test rig. The dead band clearance is similarly observed during carbide tests at 127 µm clearance and reinforced thermoplastic I tests, but not during reinforced thermoplastic II tests. A bent-shaft excitation

could also contribute to the apparent dead band clearance. Figure 6-6 shows forces recorded by load cells at the seal match XLTRC2 prediction of roughly 60 N of synchronous support. Super-synchronous components account for differences between predicted and measured force.

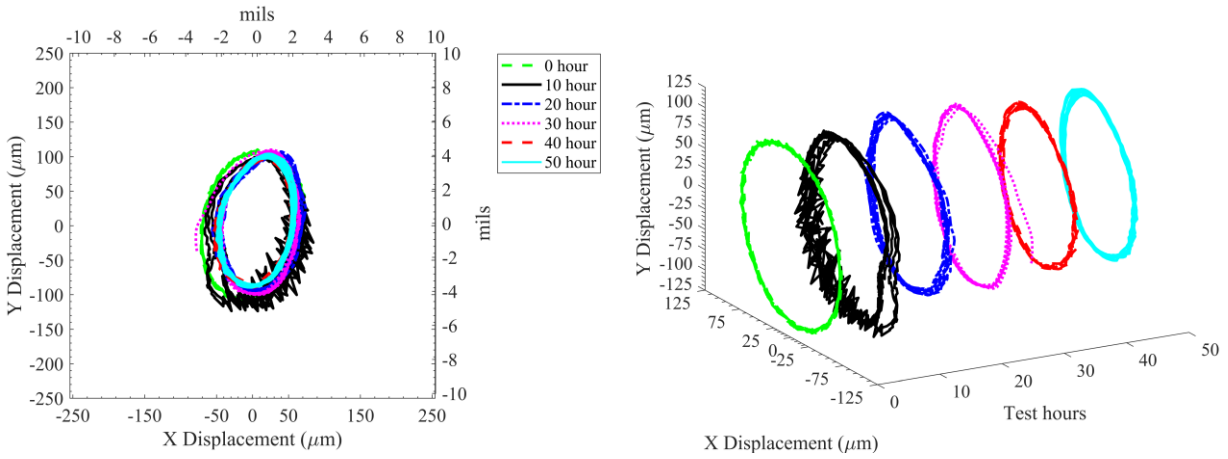

Figure 6- 3 Unbalanced disk vibrational orbit response over the duration of SiC test 1 (0 % GVF) with an initial radial clearance of 15 µm

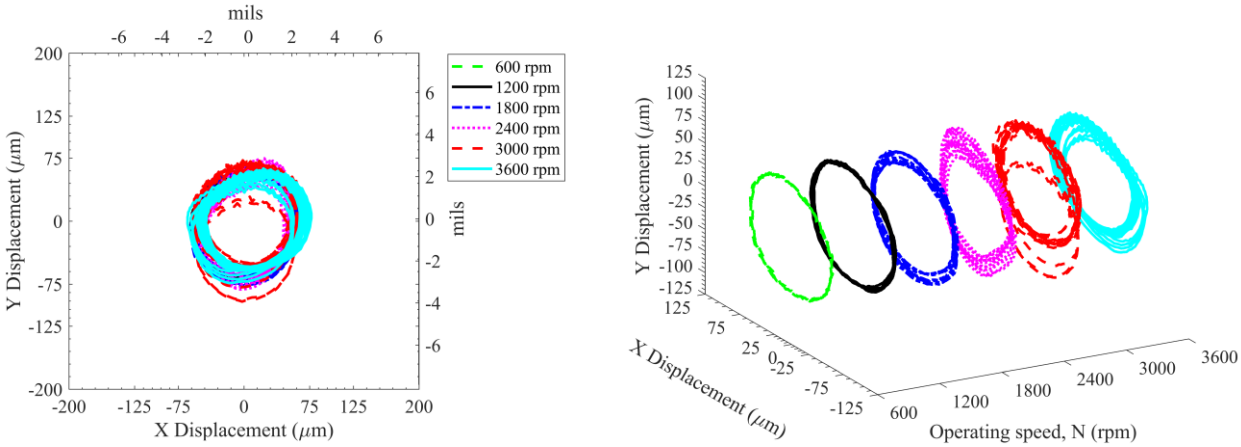

Figure 6- 4 Unbalanced disk vibration orbits at the start of SiC test 3 (80% GVF) with an initial radial clearance of 15 µm

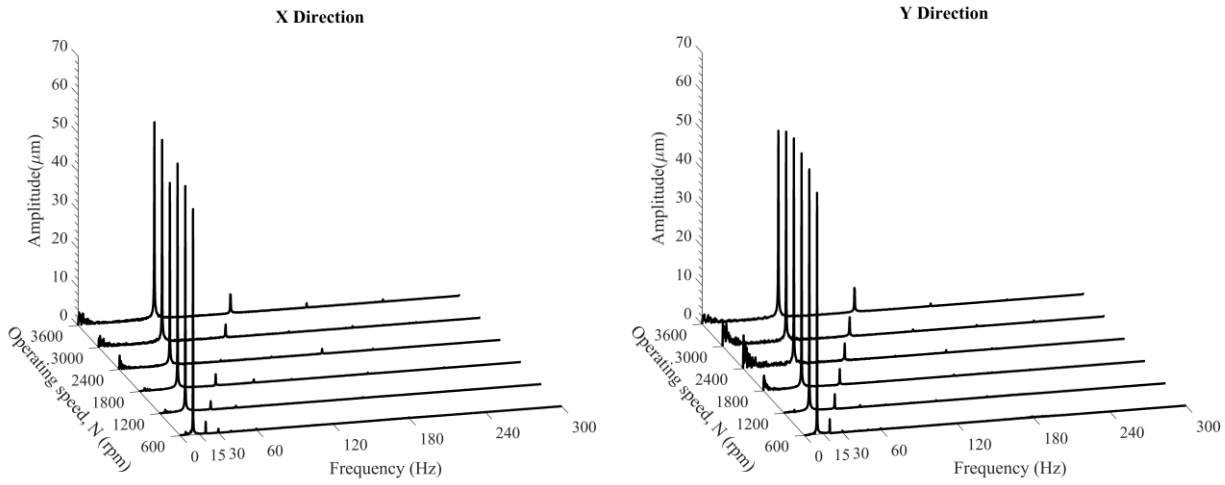

Figure 6- 5 Proximity probe waterfall plots at the beginning of SiC test 3 (diamond coated 80% GVF) with an initial radial clearance of 15 µm

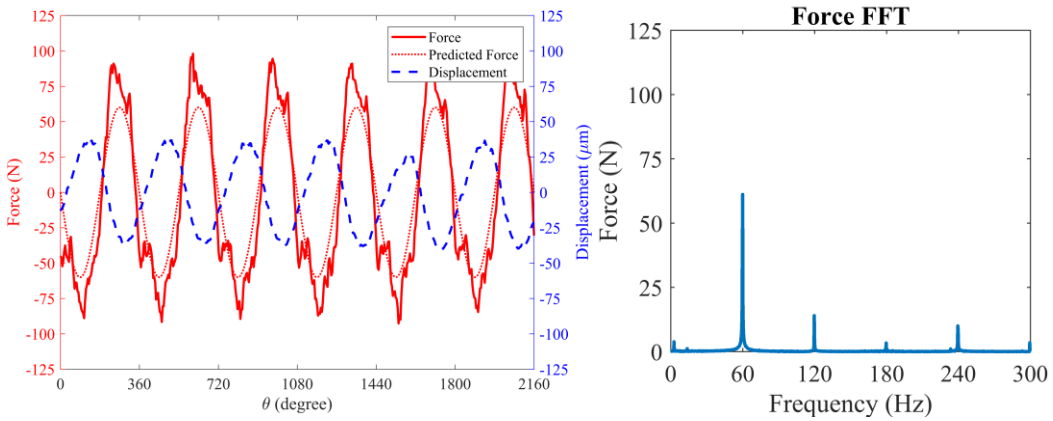

Figure 6- 6 Force data at the start of SiC test 2 (80% GVF) with an initial radial clearance of 15 µm. Measured force differs from XLTRC2 force predictions due to high frequency components.

Figures 6-7 & 6-8 show varying GVF minimally impacts the vibration orbit diameter when GVF is varied briefly during testing. Figure 6-8 shows vibration orbital response varies greatly due to low frequency vibrations when GVF increases. The low frequency vibrations occur around 5 Hz without a distinct frequency. Low frequency vibrations may result from

acoustic resonance from mixed flow through the seal and a lower sound speed, as theorized by San Andrés and Lu [37]. The low frequency vibrations may also be related to rub within the seal.

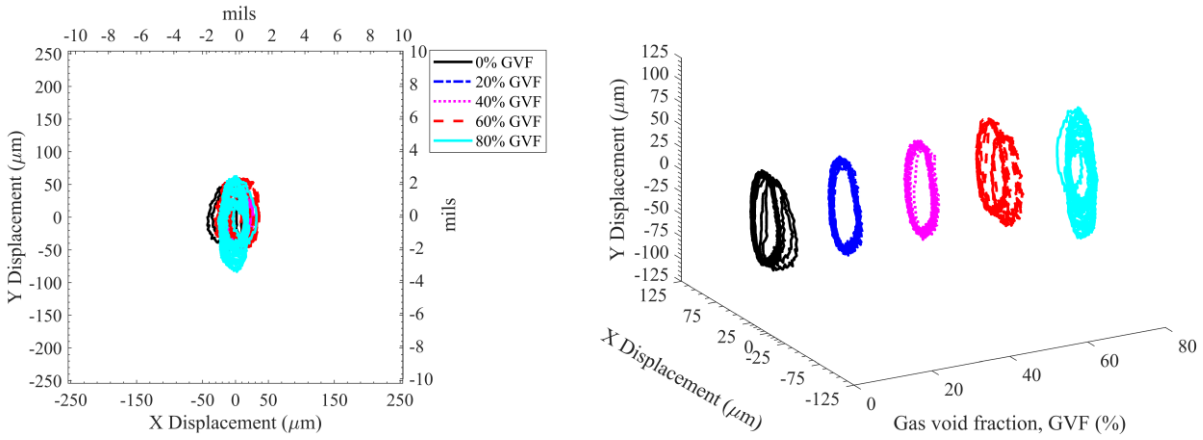

Figure 6- 7 Unbalanced disk vibration orbit at different GVFs during test 4 after 30 hours of operation with an initial radial clearance of 15 µm

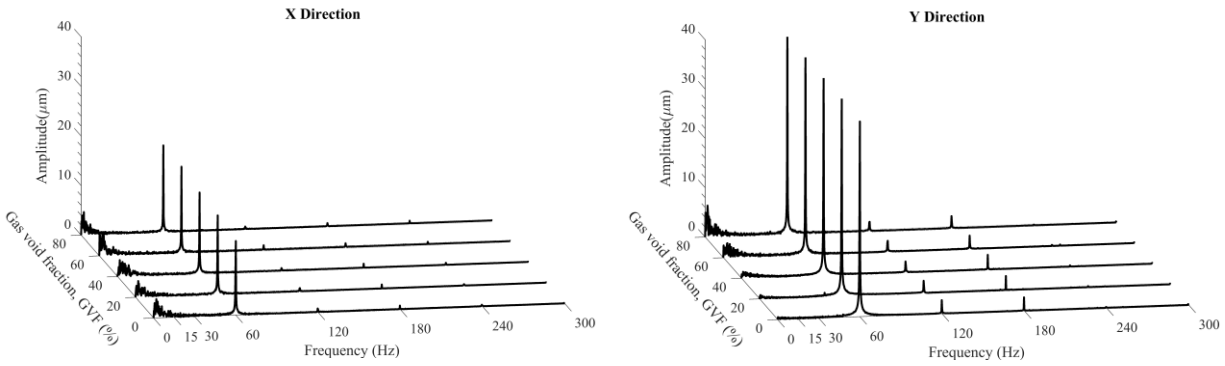

Figure 6- 8 Proximity probes FFT at different GVFs during test 4 after 30 hours of operation with an initial radial clearance of 15 µm

Inspection images of the seal and sleeve in Figs. 6-9 & 6-10 reveal polishing and faint circumferential grooves concentrated around the inlet of the seal and sleeve. Greater polishing occurrs on a 120^{o} portion of the SiC sleeves. Based on the minimal wear and minimal circumferential grooves, the majority of sand passed directly through the axial grooves. SiC seals are highly resistant to sliding wear under water lubrication, in line with tests performed by Andersson [26].

Polishing decreases the coefficient of friction and the film thickness required to prevent sliding wear. Polishing on a 120^{o} portion of the shaft sleeve indicates non-stationary contact occurred, where the point of contact between the shaft and seal rotate around the seal with the rotor unbalance. Unlike tungsten carbide seals tested by Morrison et al. [4], SiC materials exhibited no signs of heat checking.

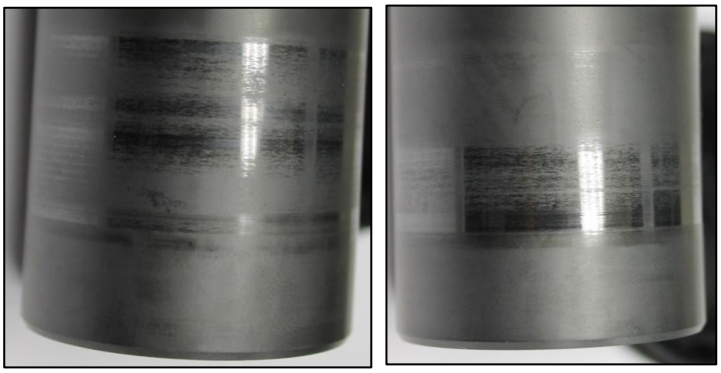

Figure 6- 9 Sleeve polishing after 100 hours of operation from SiC test no. 4 with an initial radial clearance of 15 μm

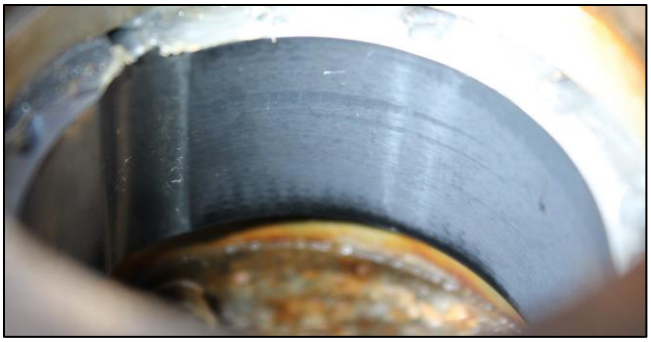

Figure 6- 10 Seal polishing after 50 hours of operation from SiC test no. 4 with an initial radial clearance of 15 µm

SiC tests with an initial clearance of 15 µm commonly produced fractures. Press fitting a collar around the seal for testing fractured two seals; an alternative method with set screws eliminated the need for press fitting. Two of the four tests ended with fractures during disassembly, as shown in Table 6-2. Figure 6-11 shows when fracture occurred, cracks propagated throughout the entire seal or sleeve. Fracture resulted in the component breaking into numerous pieces with some chalky particles. Leakage was minimal and varied little during testing at constant GVF. Test no. 1 at 0% GVF produced a leakage rate of roughly 23 LPM throughout testing.

Table 6- 2 Fracture report from SiC tests with an initial radial clearance of 15 µm

No.	Coating	GVF (%)	Fracture Notes
1.	None	0	No fracture
2.	None	80	Sleeve and seal fracture after 50 hours
3.	Diamond	80	No fracture
4.	None	40 for 50 hours, 80 for 50 hours	Seal fracture after 100 hours

a) Test 2 fracture b) Test 4 fracture

Figure 6- 11 SiC fracture images

6.2 Carbide tests with 127 µm initial radial clearance

Table 6-3 lists tests performed on SiC and WC seals with an initial radial clearance of 127 µm. Test conditions are listed in the experimental facilities section. Tests are conducted with sand concentrations matching other tests (0.057 g/L) as well as with ten times the sand concentration of other tests. The purpose of testing with higher sand concentrations is to increase wear rate and identify wear mechanisms.

Table 6- 3 Carbide test matrix with 127 µm initial radial clearance

No.	Material	Geometry	GVF (%)	Sand Concentration (g/L)
1.	SiC	Plain	0	0.057
2.	SiC	Grooved	0	0.057
3.	SiC	Plain	0	0.57
4.	WC	Plain	0	0.57

Figure 6-12 shows the radial clearance as a function of test hours. Axial grooves negligibly impact wear rate. Higher sand concentrations slightly increase wear rate, but not by an appreciable amount. This suggests the majority of wear results from sliding wear rather than three-body abrasion. WC performs slightly better than SiC, but by a negligible amount of roughly 20 µm over 50 hours. Figure 6-13 shows wear is distributed between the seal and shaft sleeve.

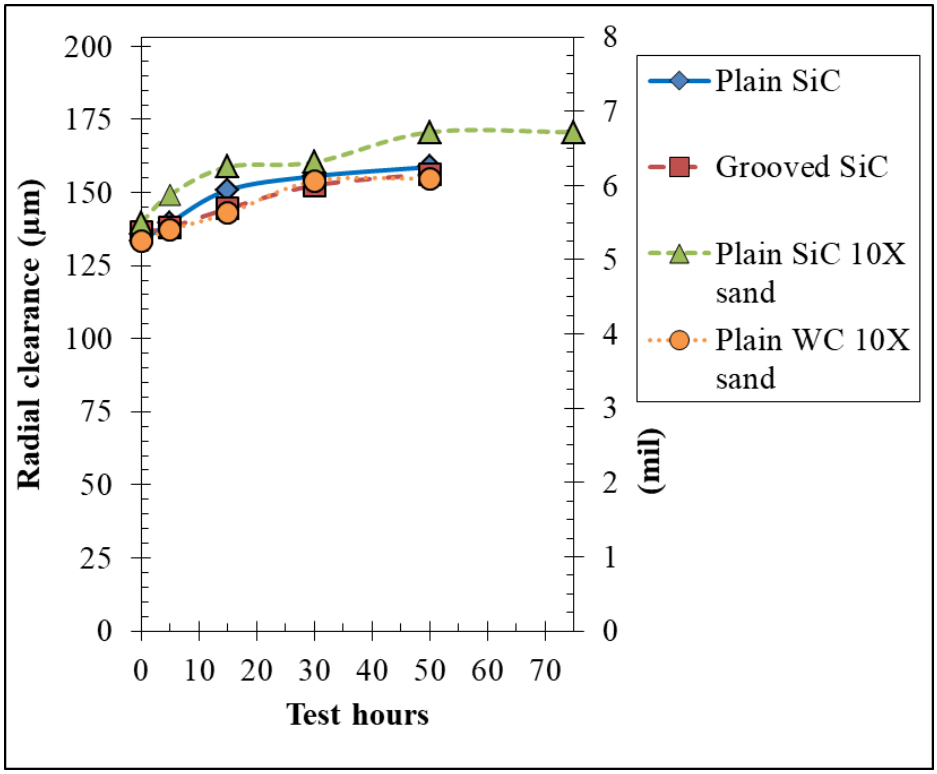

Figure 6- 12 Radial clearance as a function of test hours for carbide tests with an initial radial clearance of 127 µm

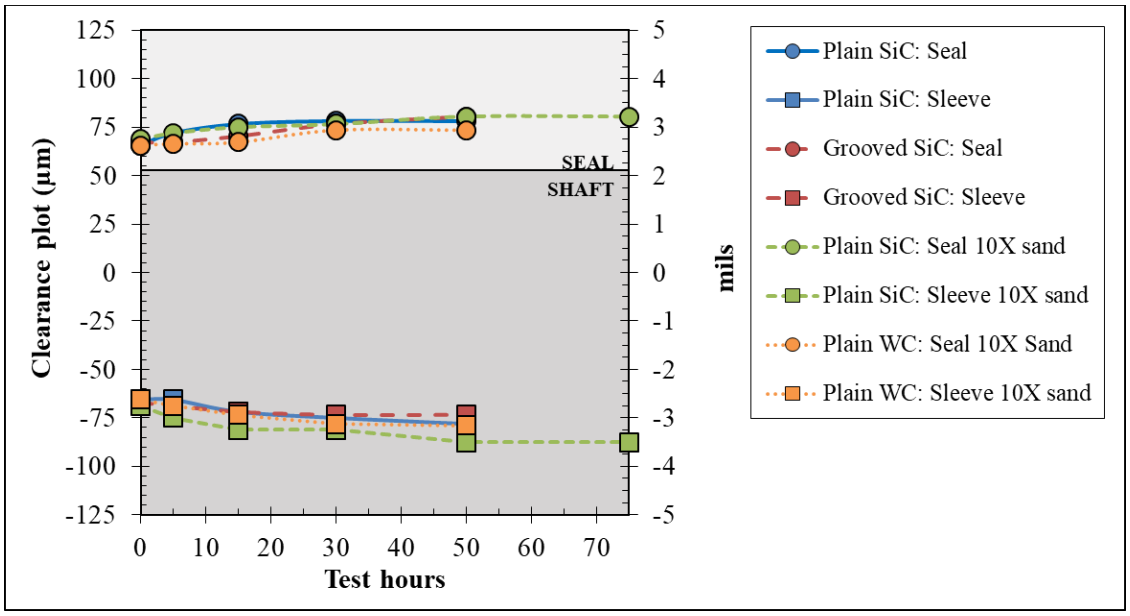

Figure 6- 13 Radial clearance as a function of seal and shaft sleeve wear for carbide tests with an initial radial clearance of 127 µm

The presence of axial grooves significantly increases leakage. The plain seal exhibited a leakage of roughly 11 LPM throughout testing, while the grooved seal exhibited a leakage of 30 LPM. Increased leakage decreases pump performance.

Two SiC tests resulted in minor seal fractures. Figure 6-14 shows the fixture holding the seal prevented large portions of the seal from breaking apart until removal from the support fixture. Test no. 2 was continued after discovering cracks during the 5 hour inspection. Over the course of the test, water passing through the seal slowly removed chips around the cracks. The remainder of the seal performed as expected and produced minimal wear. This shows SiC seals with proper support can be operated after fracture for a period of time.

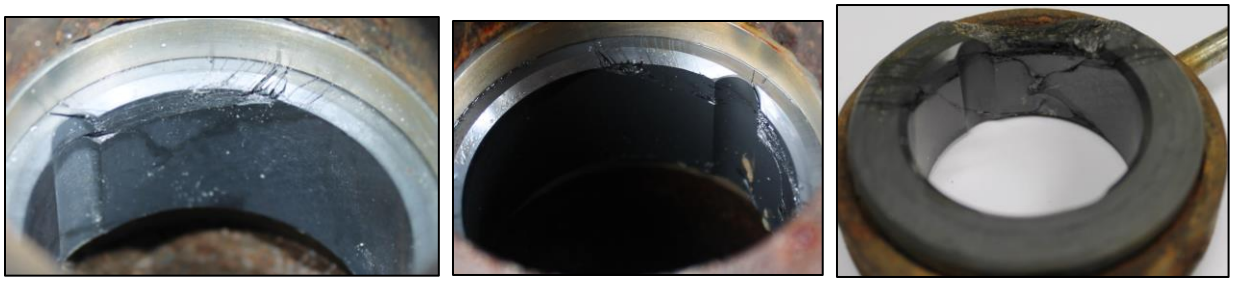

a) 5 hour inspection b) 50 hour inspection c) removal from test fixture

Figure 6- 14 SiC test no. 2 with an initial radial clearance of 127 um. Cracks developed into grooves as water removed chips. Seal remained functional.

Figure 6-15 shows SiC and WC seals and shaft sleeves developed polishing and fine circumferential grooves over the course of testing. Some larger grooves due to three-body abrasion developed near the entrance of the seal on tests with high sand concentration. This indicates three-body abrasion may become significant at even higher sand concentrations; however, three-body abrasion did not significantly impact wear rate shown in Fig. 6-12.

The WC seal and shaft sleeve developed fine axial cracks in and around polished sections not visible to the naked eye, as shown in Fig. 6-16. Morrison et al. [4] observed similar behavior on the WC shaft sleeves within interstage seals during tests of three stages of an ESP. Morrison et al. theorize subsurface cracks develop from heat checking, which become exposed when material is removed during polishing. SiC seals did not develop axial cracks.

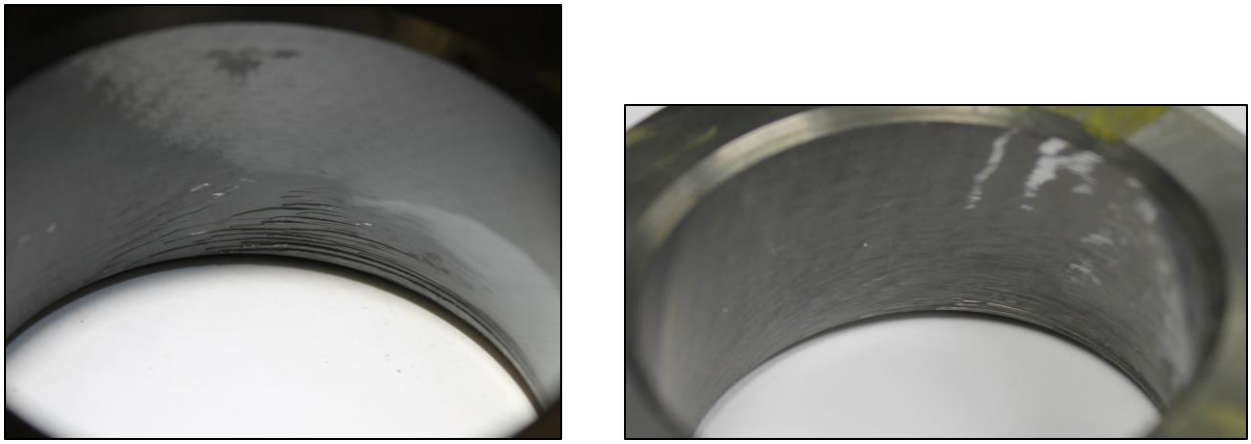

a) SiC seal after 75 hours of operation (test 3) b) WC seal after 50 hours of operation (test 4)

Figure 6- 15 Seal inspection images at the end of tests with high sand concentrations. Some large grooves developed near the inlet due to three-body abrasion, which did not significantly impact wear rate. Three-body abrasion may become significant at even higher sand concentrations.

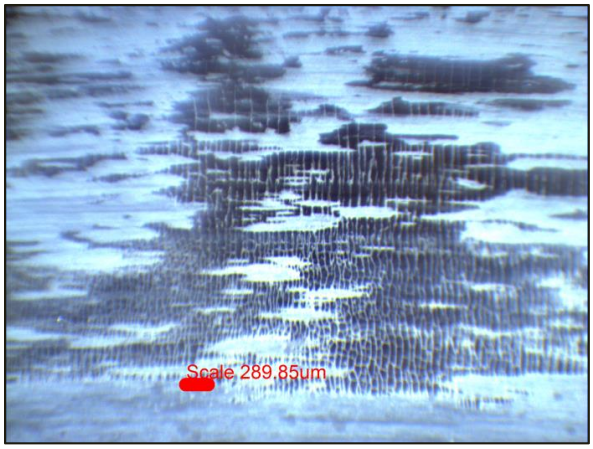

a) Shaft sleeve after 5 hours of operation

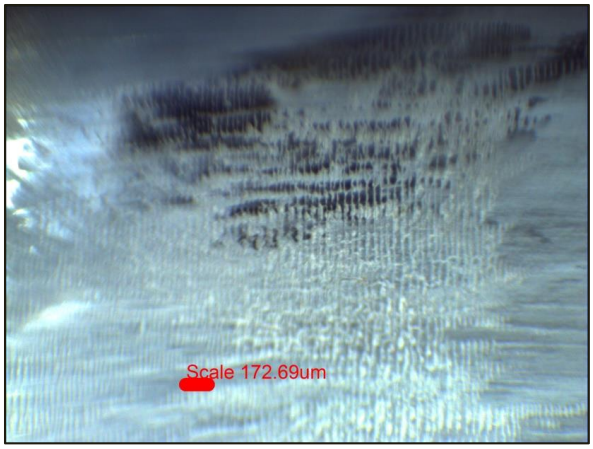

b) Shaft sleeve after 50 hours of operation

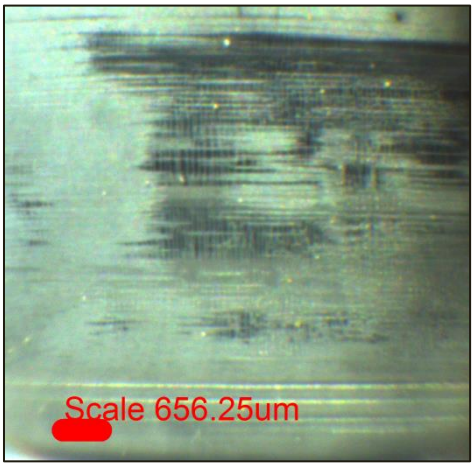

c) Seal after 50 hours of operation

Figure 6- 16 WC shaft sleeve and seal microscope inspection images. Fine axial cracks appear in and around polished regions.

6.3 Reinforced thermoplastic I tests

Burak Ayyildiz, Wenjie Yin, and Robert Hure conducted reinforced thermoplastic I tests using the component test rig discussed in section 3. Results have not been previously published. Table 6-4 lists tests conducted on reinforced thermoplastic I. Test conditions are listed in the experimental facilities section.

Table 6- 4 Reinforced thermoplastic I test matrix

No.	Grooves	GVF (%)	Notes
1.	Plain	0	
2.	Grooved	0	
3.	Plain	30	
4.	Grooved	30	
5.	Plain	60	
6.	Grooved	60	Test conducted without sand
7.	Grooved	0	

Figure 6-17 shows wet clearance as a function of test hours. Initial radial clearances are roughly 100 µm less than the median sand particle size, making sliding wear the predicted mechanism at the beginning of testing. Wear rate started slow, then accelerated as clearances increased to allow three-body abrasive wear. Wear rate decreases at higher clearances when shaft deflections are no longer large enough relative to the clearance to crush sand and produce three-body abrasion, making slurry erosion the dominant wear mechanism. Grooved seals failed to perform better than plain seals, experiencing comparable wear.

Test no. 6 was conducted without sand to determine wear patterns in the absence of three-body abrasion. This test produces similar wear rates for clearances below sand particle sizes, but wear rate decreases once clearances reach sand particle sizes. Results from the test without sand suggest that in the presence of sand, sliding wear is the dominant wear mechanism at tight clearances while three-body abrasion is the dominant mechanism for clearances greater than sand particle sizes.

Increased GVF produces similar wear rates for sliding wear, but modestly accelerates three-body abrasion. The presence of air decreases force coefficients and increases shaft deflections, allowing three-body abrasion to occur at larger clearances. Slurry erosion produces similar wear rates at different GVFs.

Figure 6-18 shows dividing total wear into seal and sleeve wear reveals the seal wore slightly more than the sleeve. This is likely caused by the difference in hardness between the stainless steel sleeve and reinforced thermoplastic I seal.

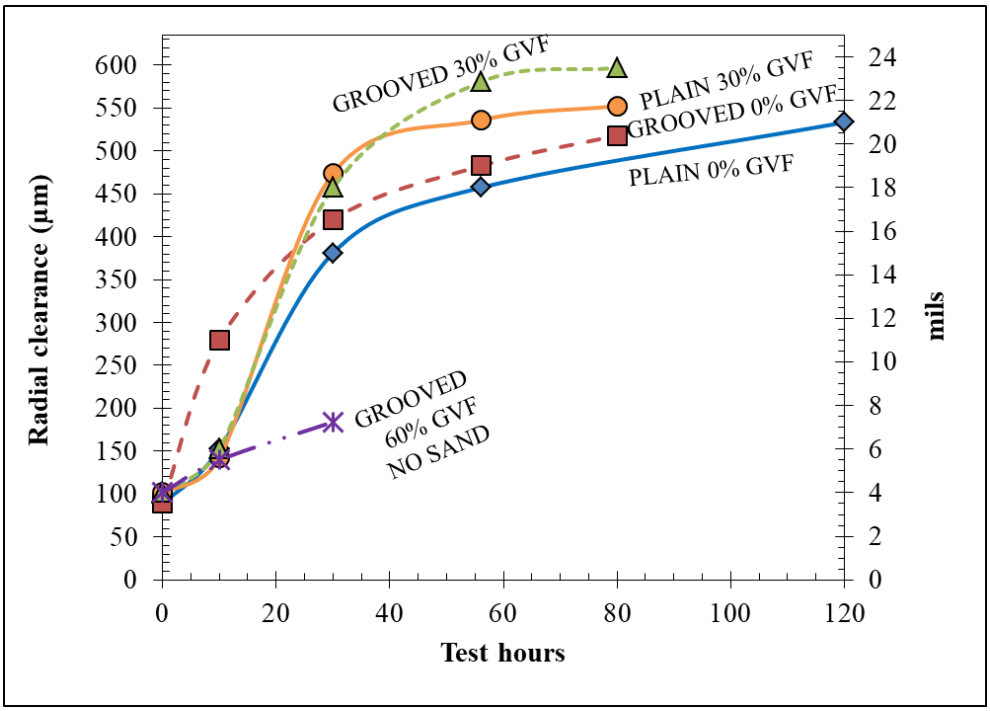

Figure 6- 17 Wet radial clearance as a function of test hours for reinforced thermoplastic I tests

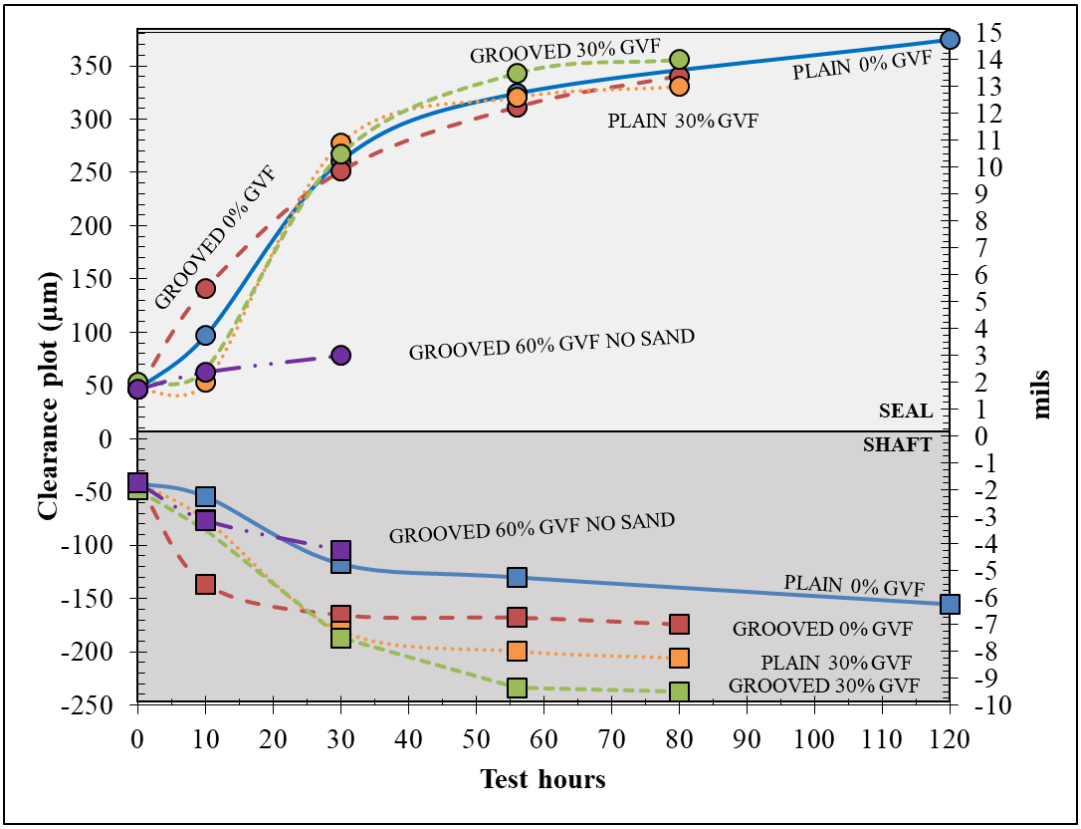

Figure 6- 18 Wet radial clearance as a function of seal and shaft sleeve wear for reinforced thermoplastic I tests

Figure 6-19 & 6-20 show clearances change significantly during the course of testing, which significantly impacts the unbalanced disk vibration orbit diameter. Vibration orbit diameter increased throughout the duration of the test. Vibration responses resemble a rounded square for grooved and plain seals at 0% GVF. Filtering out the 3X vibration component transformed vibration orbits from rounded squares to circles. A 3X vibration component is typically associated with coulomb friction or rubbing, which could have occurred between the shaft and a secondary seal above the proximity probes or from worn roller bearings. Vibration orbit diameters are consistent with XLTRC2 predictions at measured clearances.

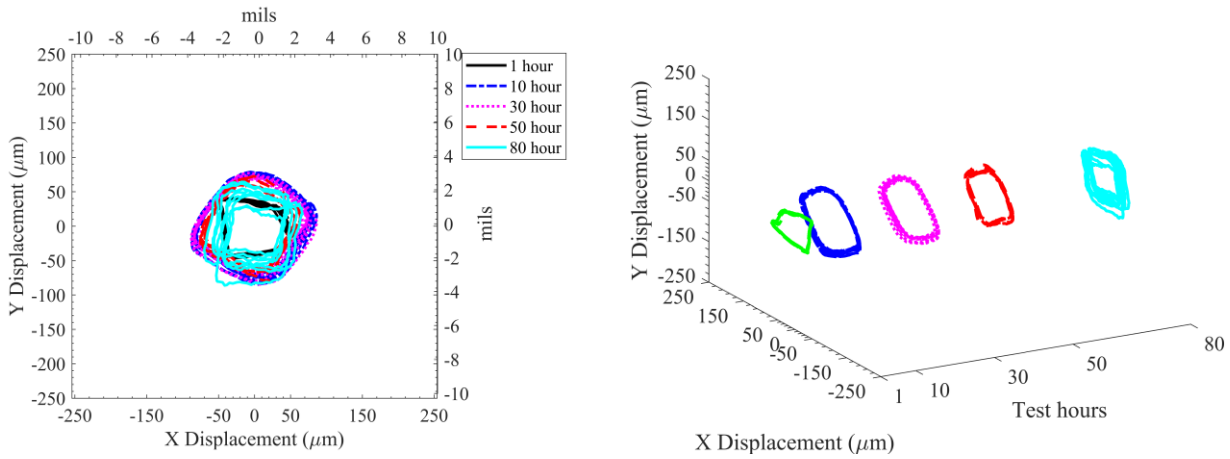

Figure 6- 19 Unbalanced disk vibration orbits from reinforced thermoplastic I test 2 at 0% GVF with grooves

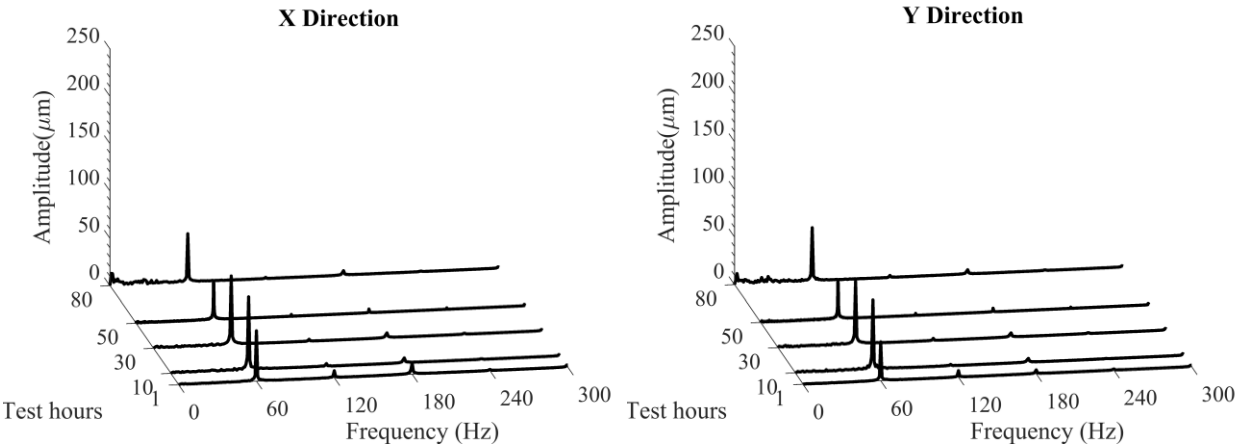

Figure 6- 20 Proximity probes FFT from reinforced thermoplastic I test 2 at 0% GVF with grooves

Figures 6-21 through 6-24 show increased GVF adds variability to the vibration orbit through low frequency vibrations. The low frequency vibrations occur around 15 Hz, although there is not a distinct frequency. Similar vibrations occur at 0% GVF with large clearances. Low frequency vibration responses were unaffected by the absence of sand.

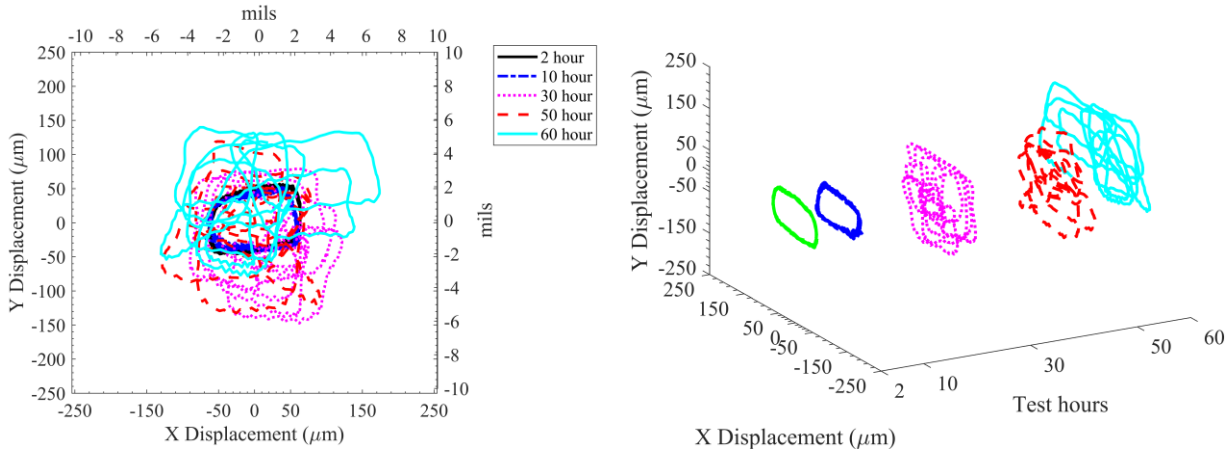

Figure 6- 21 Unbalanced disk vibration orbits from reinforced thermoplastic I test 3 at 30% GVF without grooves

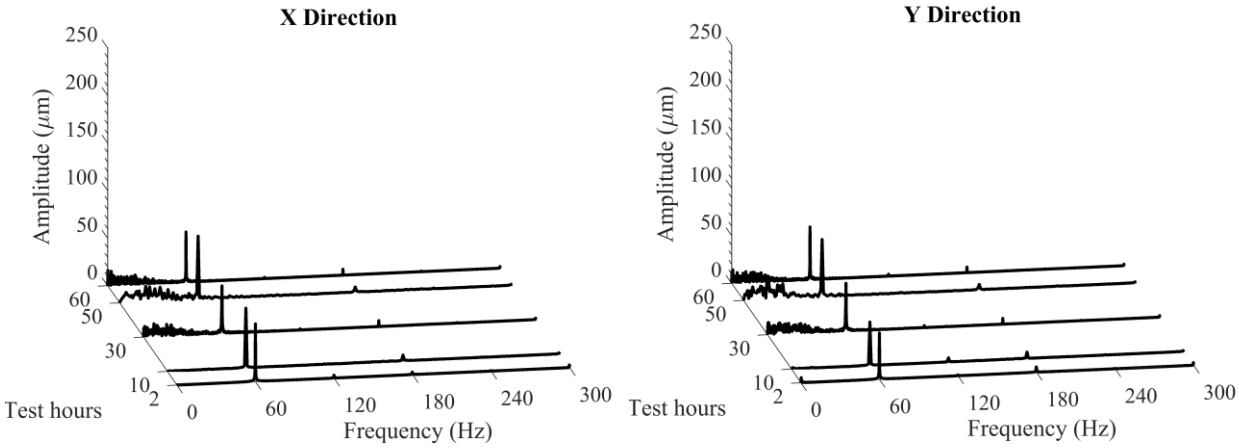

Figure 6- 22 Proximity probes FFT from reinforced thermoplastic I test 3 at 30% GVF without grooves

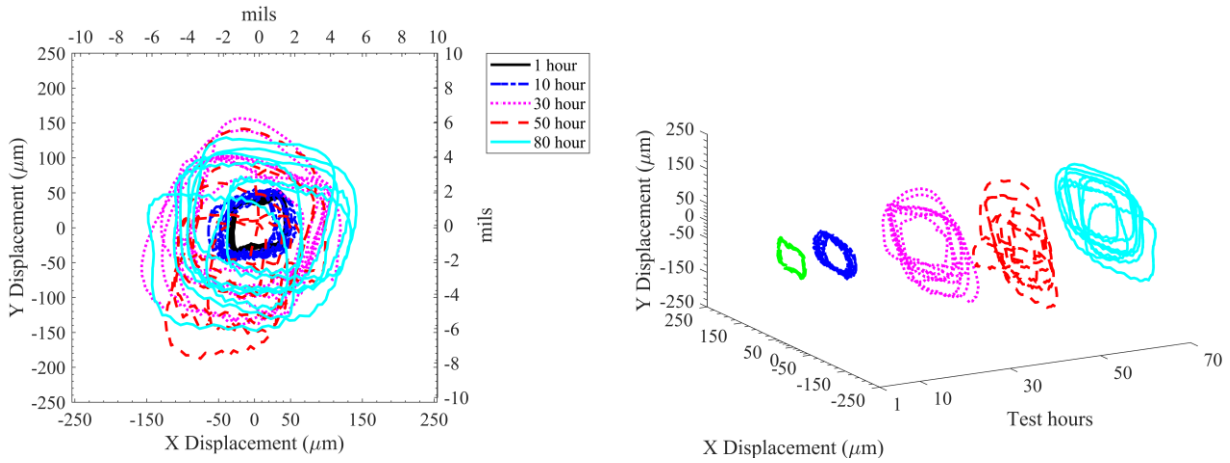

Figure 6- 23 Unbalanced disk vibration orbits from reinforced thermoplastic I test 4 at 30% GVF with grooves

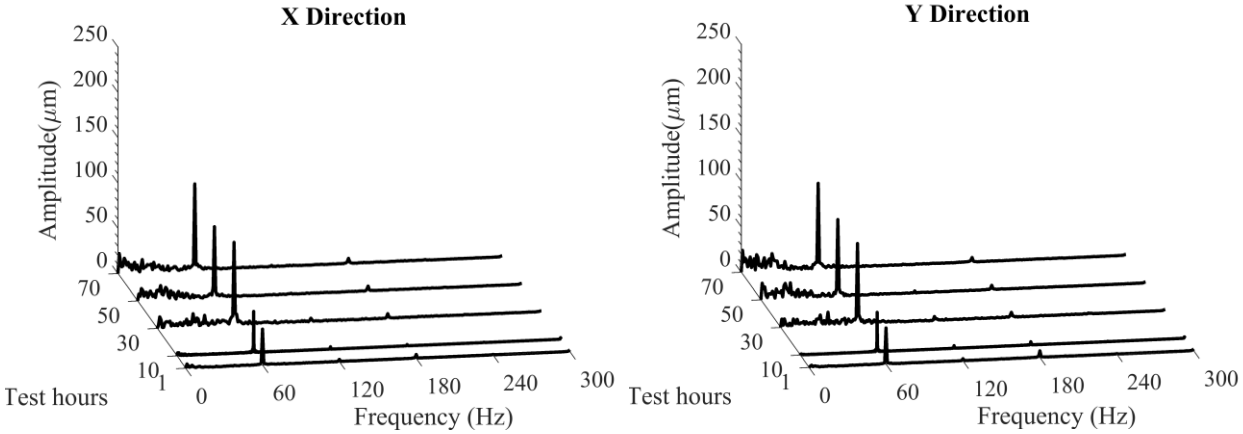

Figure 6- 24 Proximity probes FFT from reinforced thermoplastic I test 4 at 30% GVF with grooves

Microscopic examination of the seals and sleeves in Figs. 6-25 & 6-26 reveal the formation of circumferential grooves from three-body abrasion during testing. Slurry erosion wore away circumferential grooves once clearances increased enough to allow the passage of uncrushed sand. Figure 6-27 shows heat stains, particularly on the shaft sleeve, indicate heat checking occurred at high GVFs. Increasing GVF decreased convective heat transfer and enhanced heat checking. Axial cracks were not observed.

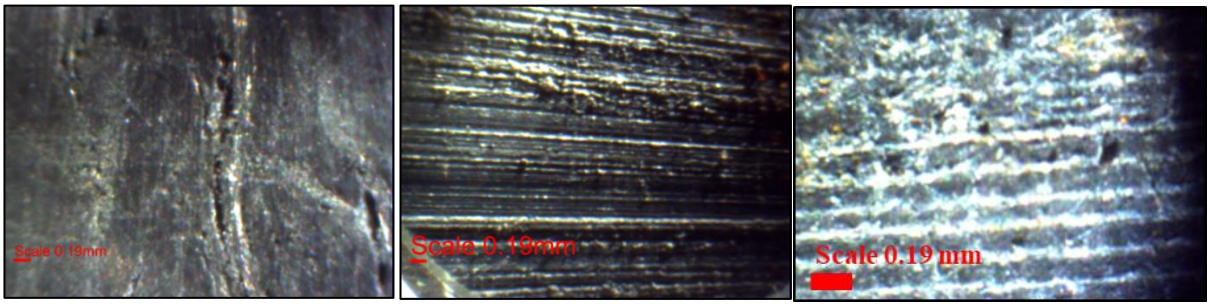

a) 0 hours b) 10 hours c) 30 hours

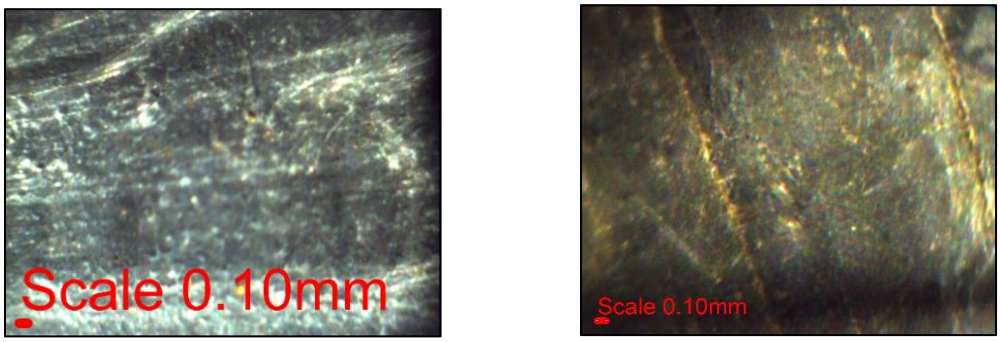

d) 56 hours e) 120 hours

Figure 6- 25 Seal microscopic inspection images of reinforced thermoplastic I test 1 at 0% GVF without grooves

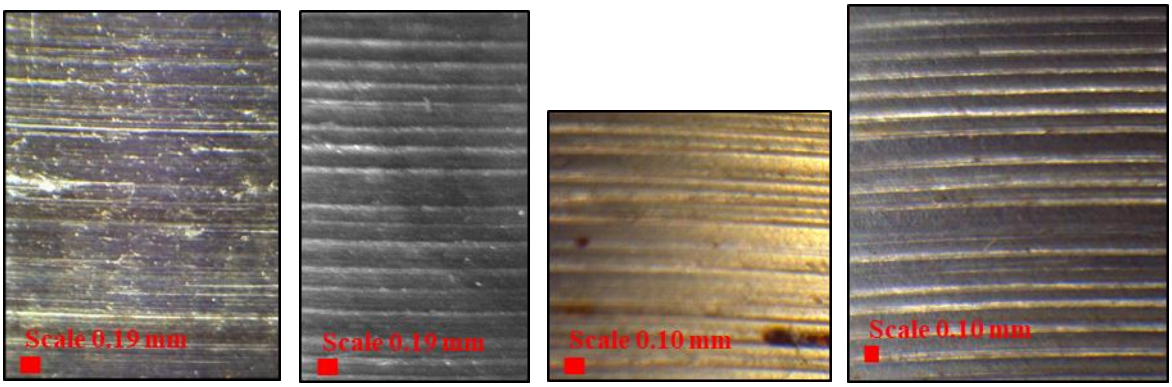

a) 10 hours b) 30 hours c) 56 hours d) 120 hours

Figure 6- 26 Sleeve microscopic inspection images of reinforced thermoplastic I test 1 at 0% GVF without grooves

a) 30% GVF sleeve (test 3) b) 60% GVF sleeve (test 5) c) 60% GVF seal (test 5)

Figure 6- 27 Inspection images of the seal and sleeve from reinforced thermoplastic I testing revealing heat checking

Severe test rig vibrations led to significant wear and the termination of two tests. Figure 6-28 shows change in radial clearance over time for terminated tests. It is hypothesized poor alignment contributed to the severe wear rate and test rig vibrations.

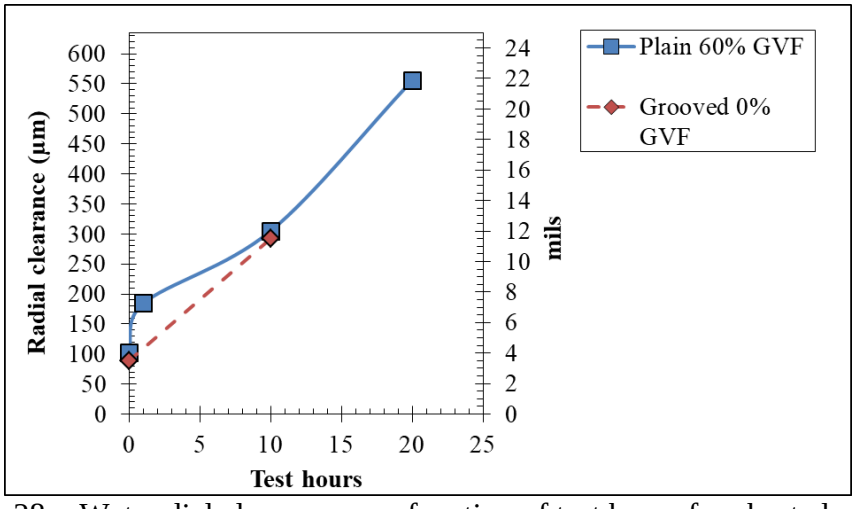

Figure 6- 28 Wet radial clearance as a function of test hours for aborted reinforced thermoplastic I tests

6.4 Reinforced thermoplastic II tests

Table 6-5 lists tests conducted on reinforced thermoplastic II, and Fig. 6-29 shows wear as a function of test hours. Test conditions are listed in the experimental facilities section. Clearances increase quickly under three-body abrasion. For tests at 0% GVF, wear rate decreases dramatically after radial clearances reach 325 μm, the predicted transition point from three-body abrasion to slurry erosion. Tests conducted without sand saw minimal wear, indicating three-body abrasion is the dominant wear mechanism at initial clearances. Figure 6-30 shows wear concentrated on the seal rather than the sleeve, which is expected based on the hardness of the seal and sleeve. Grooved seals experienced wear comparable to plain seals.

Table 6- 5 Reinforced thermoplastic II test matrix

No.	Grooves	GVF (%)	Notes
1.	Plain	0	
2.	Plain	40	
3.	Grooved	0	Initial clearance increased to 210 μm
4.	Plain	0	Test conducted without sand
5.	Plain	40	Test conducted without sand

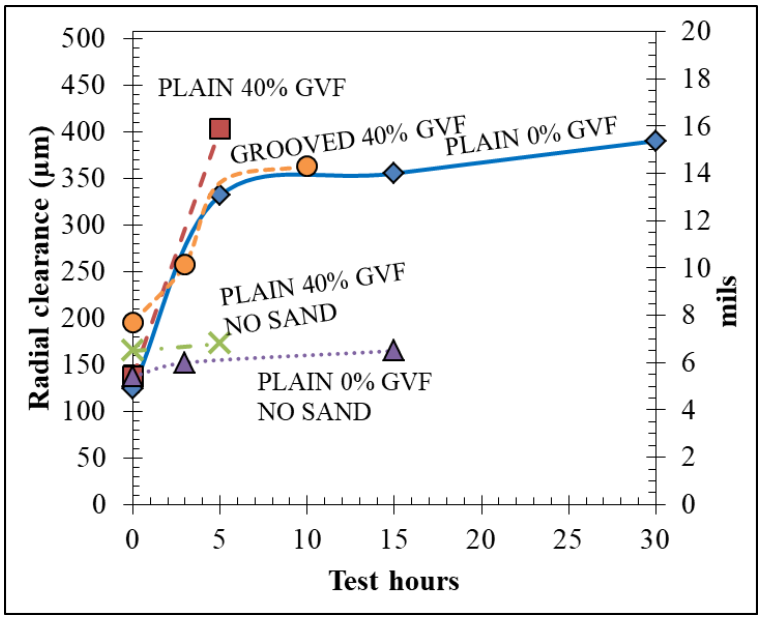

Figure 6- 29 Wet radial clearance as a function of test hours for reinforced thermoplastic II tests

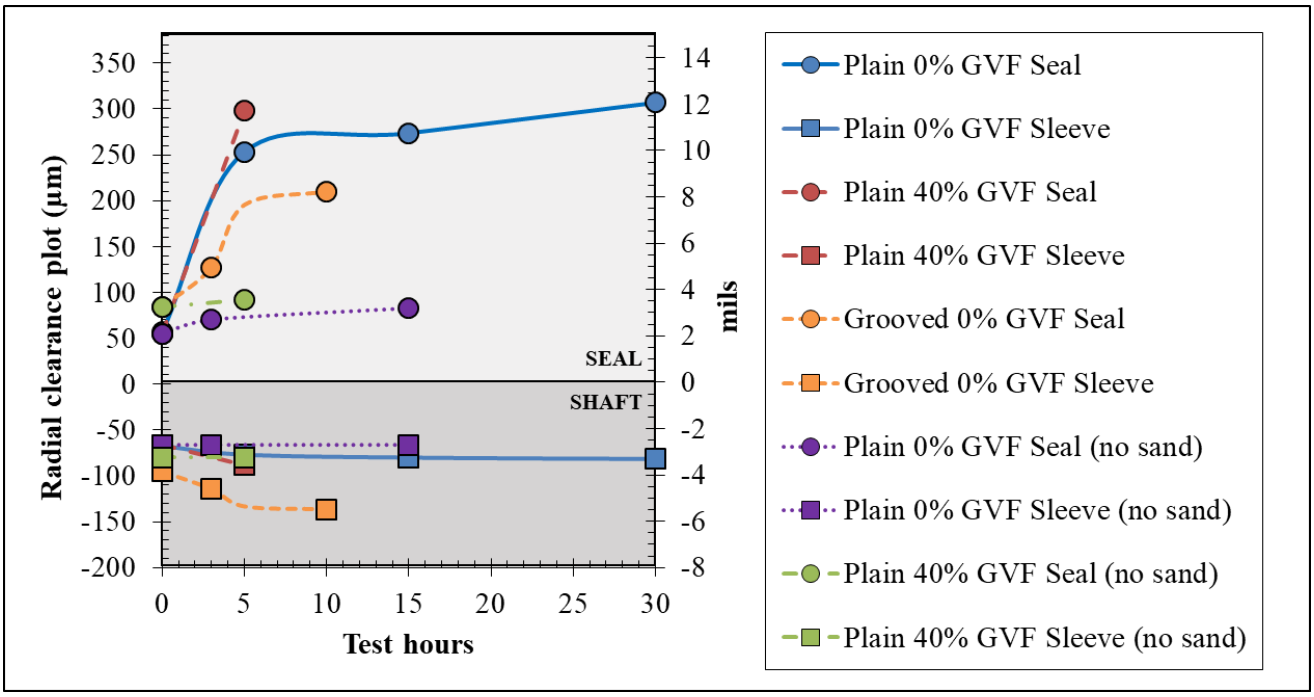

Figure 6- 30 Wet radial clearance as a function of seal and sleeve wear for reinforced thermoplastic II tests

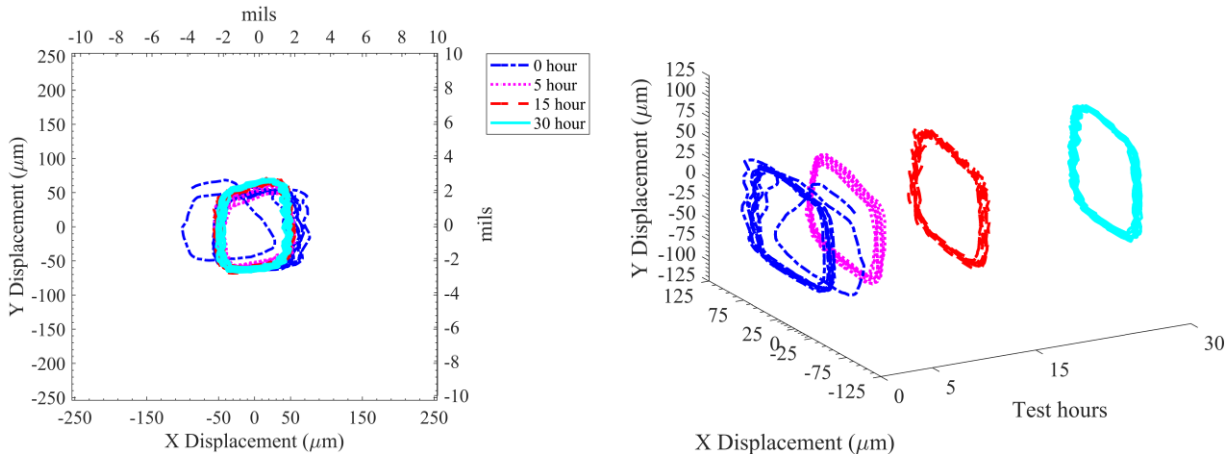

Figure 6- 31 Unbalanced disk vibration orbits from reinforced thermoplastic II test 1 at 0% GVF without grooves

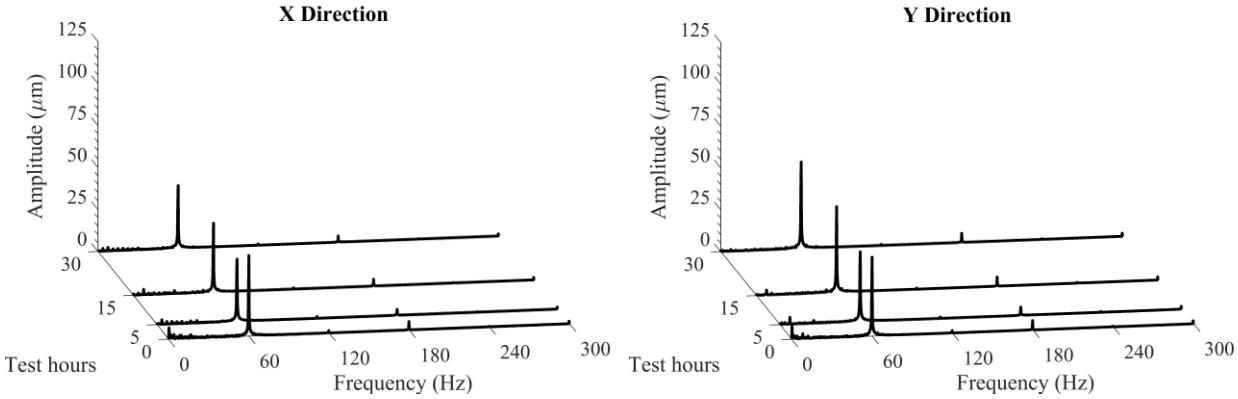

Figure 6- 32 Proximity probes FFT from reinforced thermoplastic II test 1 at 0% GVF without grooves

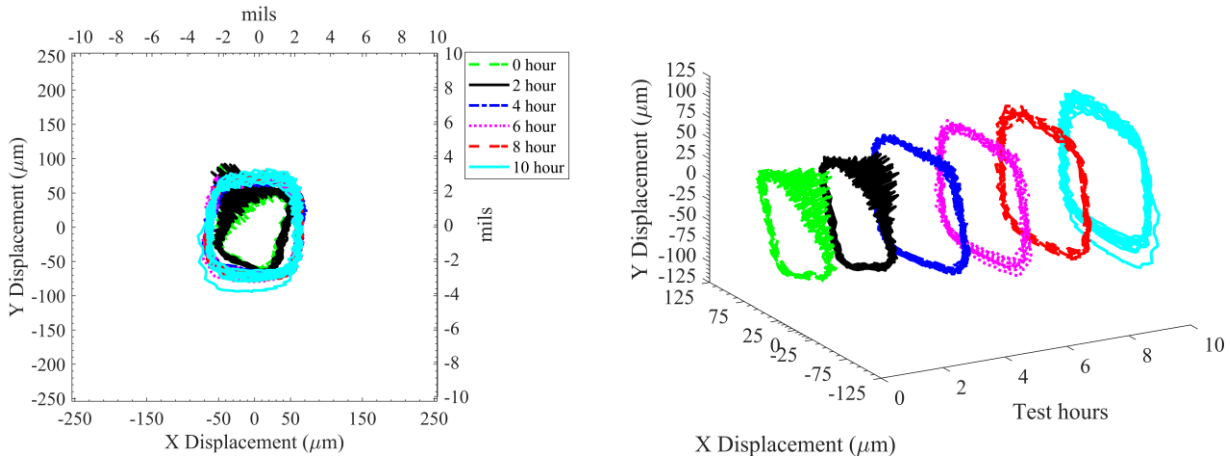

Figure 6- 33 Unbalanced disk vibration orbits from reinforced thermoplastic II test 3 at 0% GVF with grooves

Figures 6-31 through 6-34 show unbalanced disk vibration orbits resemble rounded squares for both grooved and plain seals at 0% GVF. Unbalanced disk vibration orbits change little in diameter over the course of testing, achieving large diameters immediately that are expected for clearances measured after 5 hours of operation. It is hypothesized that clearances increased rapidly due to the poor abrasive resistance of reinforced thermoplastic II, reaching large clearances by the time the rotor reached full speed. Clearances then changed little over the course of testing. Figures 6-35 & 6-36 show testing at 40% GVF produces similar results. This hypothesis is backed by leakage data, which increased from 4 LPM to 30 LPM during startup, then increased slowly to 52 LPM by the end of testing at 0% GVF.

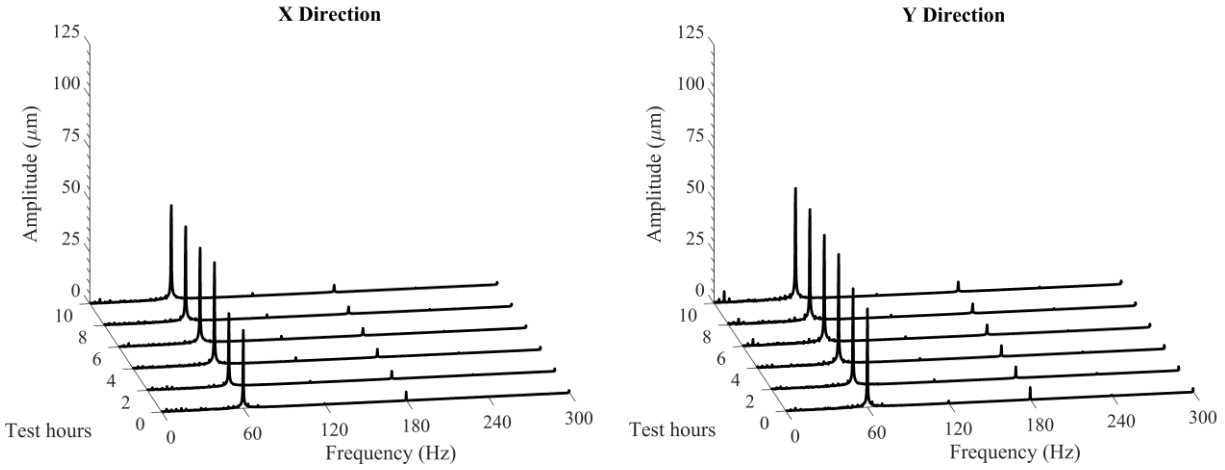

Figure 6- 34 Proximity probes FFT from reinforced thermoplastic II test 3 at 0% GVF with grooves

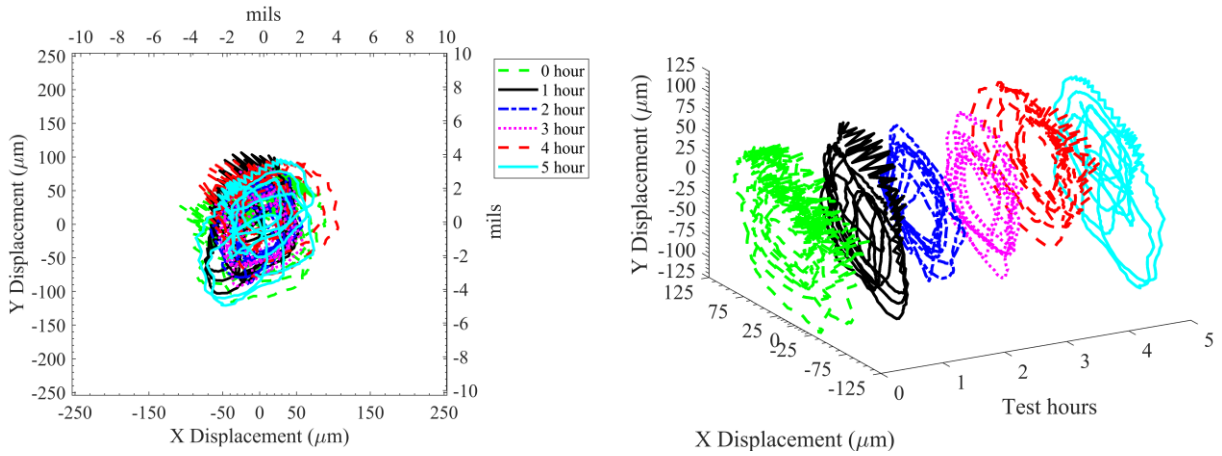

Figure 6- 35 Unbalanced disk vibration orbits from reinforced thermoplastic II test 2 at 40% GVF without grooves

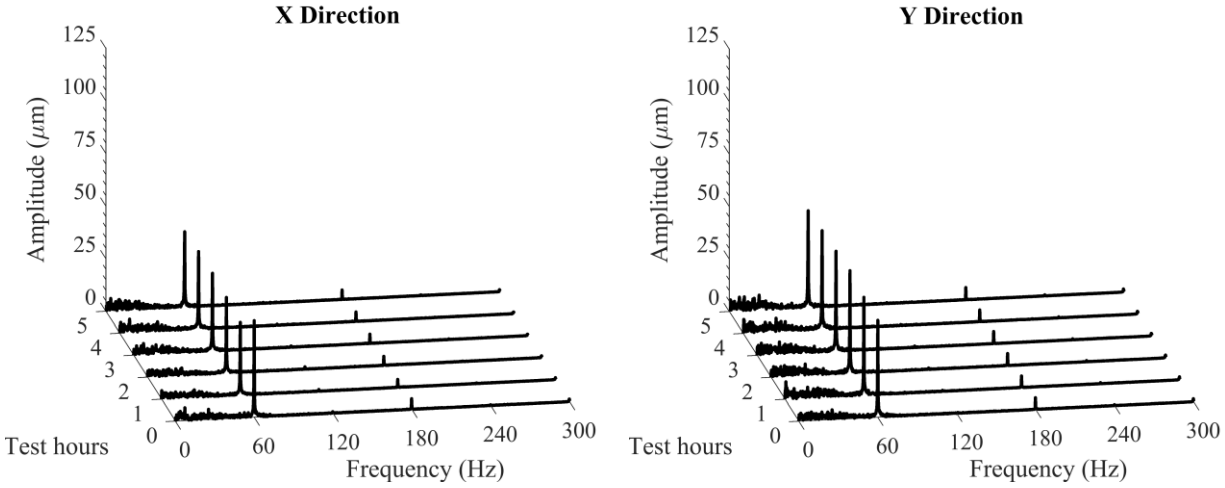

Figure 6- 36 Proximity probes FFT from reinforced thermoplastic II test 2 at 40% GVF without grooves

Inspection of test no. 2 at 40% GVF revealed the seal melted, as shown in Fig. 6-37. Water growth caused the seal to lock up when attempting to start the test. The seal was likely installed with a static eccentricity that placed the shaft sleeve within 25 µm of the seal; water growth caused impingement between the seal and sleeve, preventing rotation. In order to avoid lock up, the rotor was brought to 600 rpm with only air at 70 kPa across the seal before water

was introduced and the rotor was brought to 3600 rpm. Air produced significantly less convective heat transfer than water, allowing temperatures to exceed the material melting point of 340 ^{o}C. The flow of water pulled seal material downstream until it solidified around steel supporting the seal. The sleeve showed staining from heat checking. Inspection images displayed in Figs. 6-38 & 6-39 from test no. 2 and others show circumferential grooves from three-body abrasion. Tests at 0% GVF produced no signs of heat checking. Lock up and melting did not occur during test no. 5 when the rotor started with 40% GVF and 345 kPa across the seal.

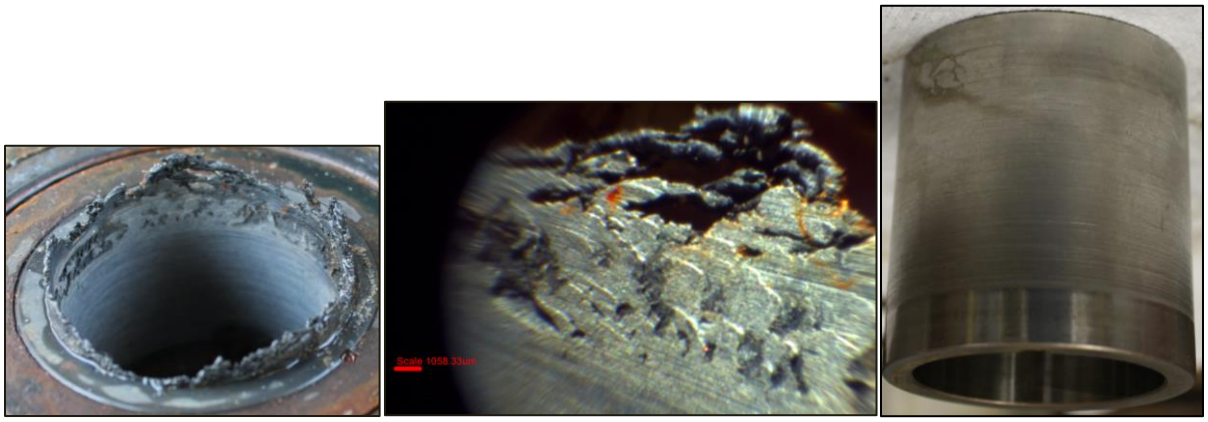

Figure 6- 37 Inspection images from reinforced thermoplastic II test no. 2 at 40% GVF

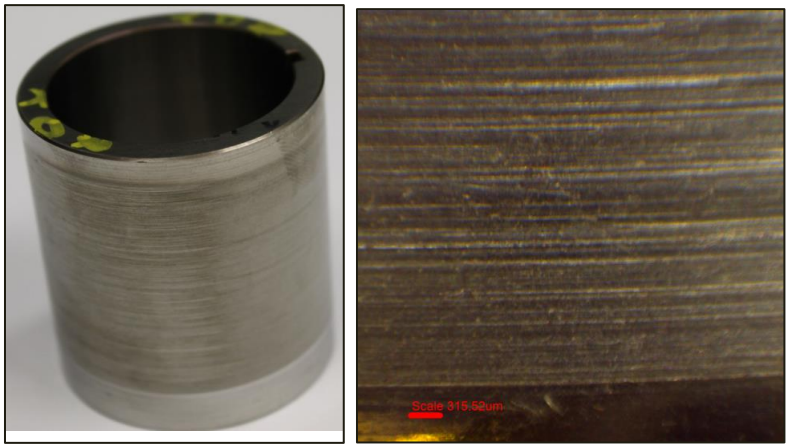

Figure 6- 38 Sleeve inspection images from reinforced thermoplastic II test no. 1 at 0% GVF

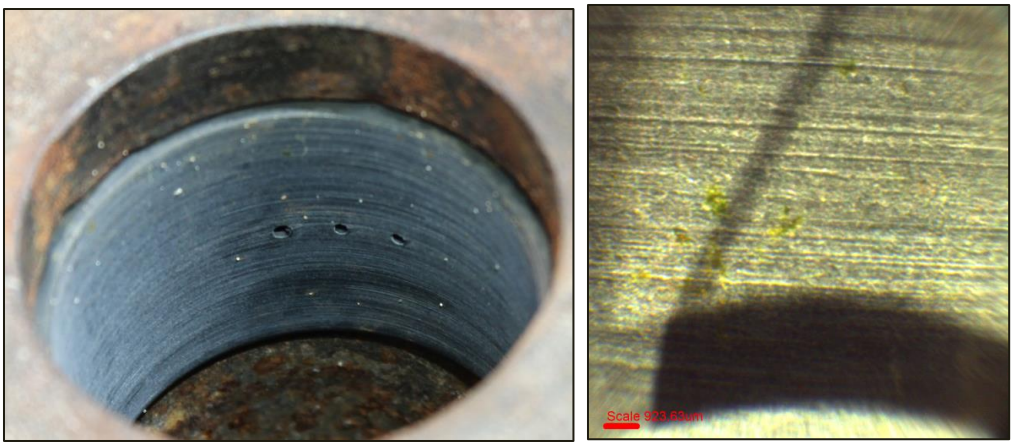

Figure 6- 39 Seal inspection images from reinforced thermoplastic II test no. 1 at 0% GVF

6.5 Material and clearance comparisons

This section presents a comparison of results from the preceding sections. Previous discussion established the ineffectiveness of axial grooves and the comparable wear of SiC and WC. This section will compare different reinforced thermoplastics, reinforced thermoplastics with SiC, and SiC with different initial radial clearances.

Figure 6-40 show a comparison between plain reinforced thermoplastics at 0% GVF. Reinforced thermoplastic I shows better wear resistance at small clearances, while reinforced thermoplastic II increases in clearance almost immediately. Reinforced thermoplastic II produced faster three-body abrasion. Figure 6-41 shows wear rate decreased at lower clearances for reinforced thermoplastic II due to less sleeve wear. This discrepancy is likely caused by greater initial misalignment during reinforced thermoplastic I tests, allowing three-body abrasion to occur at larger clearances. Based on these results, reinforced thermoplastic I exhibits superior wear resistance.

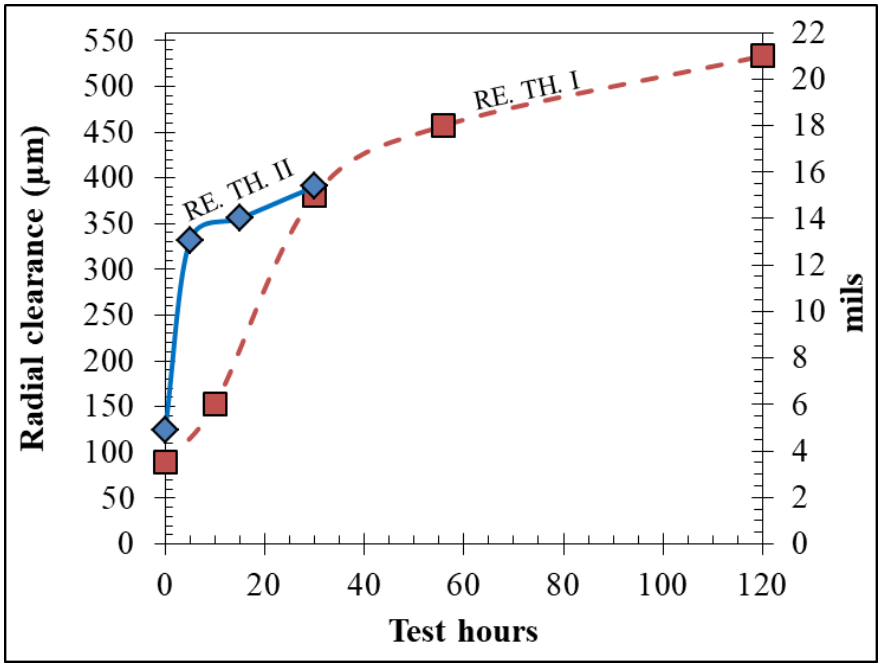

Figure 6- 40 Wet radial clearance as a function of test hours for reinforced thermoplastic tests at 0% GVF without grooves

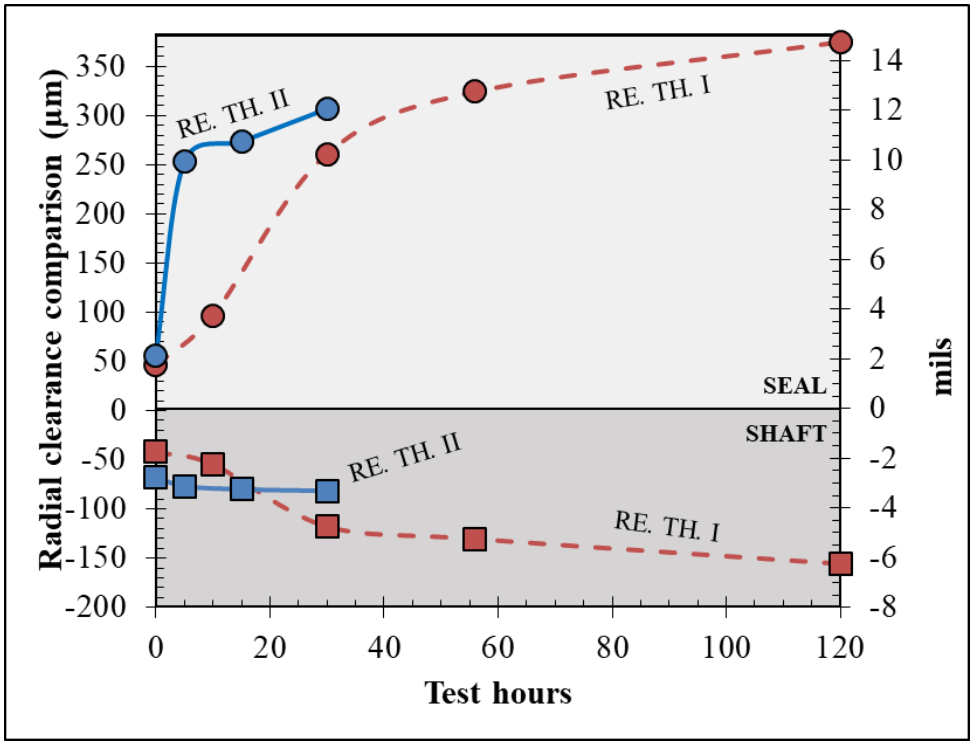

Figure 6- 41 Wet radial clearance as a function of seal and sleeve wear for reinforced thermoplastic tests at 0% GVF without grooves

Figure 6-42 shows a comparison between plain reinforced thermoplastic I and SiC with similar initial radial clearances. The superior wear resistance of SiC indicates reinforced thermoplastics are not competitive with carbides, and reinforced thermoplastics are not suitable for ESPs when sand is present.

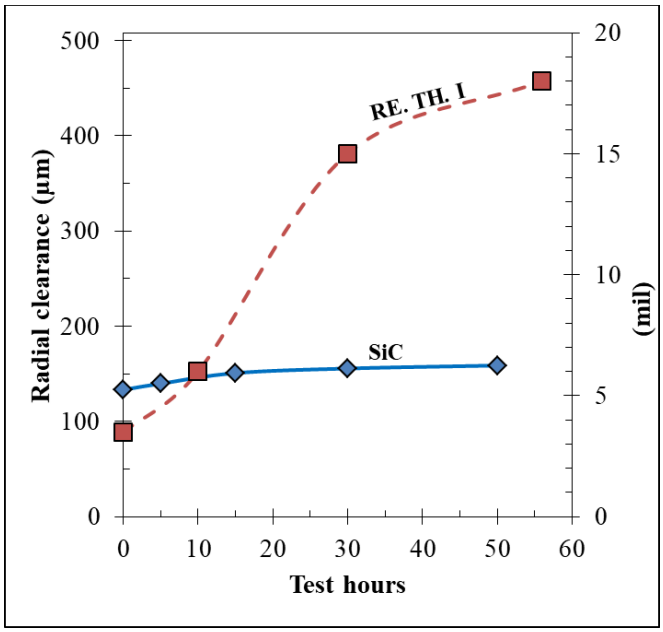

Figure 6- 42 Radial clearance as a function of test hours for plain SiC and plain reinforced thermoplastic I at 0% GVF with similar initial radial clearances

Figure 6-43 shows a comparison between grooved, 0% GVF SiC tests at different initial radial clearances. Grooved tests are presented because of the absence of plain tests at 15 µm initial radial clearance. The test at larger initial clearance produces similar wear. This result shows initial radial clearance does not significantly impact wear rate, dispelling the hypothesis that small clearances limit sand from entering the seal and creating damaging three-body abrasion. This result is consistent with the lack of change in wear rate when sand concentration

increased, denoting sliding wear as the dominant mechanism. The slight difference between the two data sets could be explained by greater sliding wear occurring at tighter clearances.

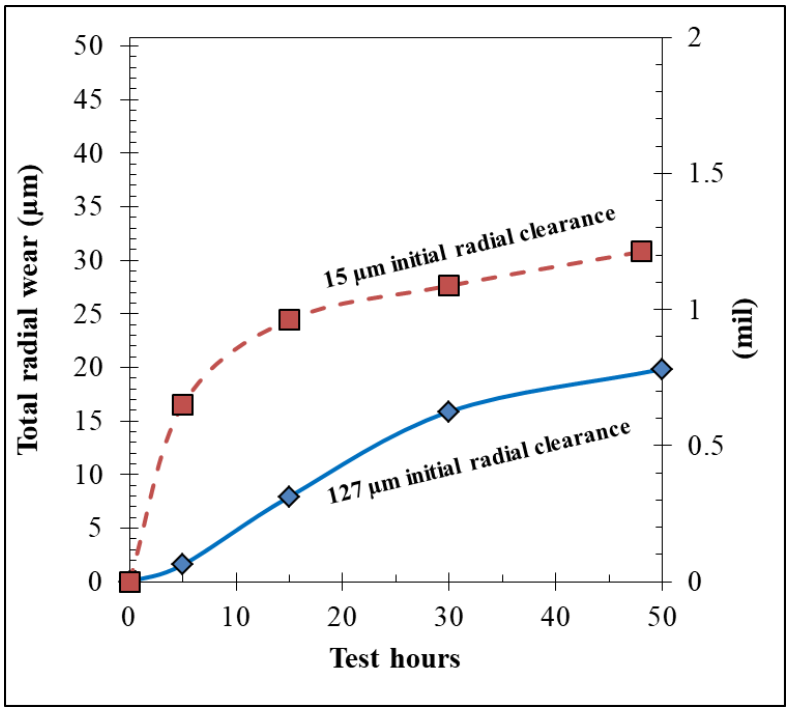

Figure 6- 43 Comparison of total radial wear for grooved SiC tests at 0% GVF with different intial radial clearances

7. CONCLUSIONS

Wear, dynamic performance, and leakage of different seals for ESPs was evaluated in a component-level test rig. Test results support the following conclusions.

Carbide seals exhibit superior wear resistance compared to reinforced thermoplastics. Reinforced thermoplastics performed well in the absence of sand, but poorly once sand was introduced. Reinforced thermoplastics are not suitable for use in ESPs where significant sand concentrations exist. Of the two reinforced thermoplastics tested, reinforced thermoplastic I is superior.

SiC and WC produced similar wear rates. WC seals and shaft sleeves developed fine axial cracks from heat checking. It is difficult to evaluate what effect these cracks have on the structural integrity of the shaft sleeve and seal, but the cracks did not produce a fracture failure. Carbide fracture failure occurred frequently.

SiC wear rate is not meaningfully impacted by initial radial clearance or sand concentration. These results imply wear was created by sliding wear rather than three-body abrasion. Prior testing by Morrison et al. [4] showed tungsten carbide seals wore from three-body abrasion with an ESP inlet sand concentration of 2.0 g/L, compared to the 0.057 or 0.57 g/L interstage seal inlet sand concentration used in these tests. One possible explanation for the different results may be different sand concentration at the inlet of an ESP and the inlet of interstage seals. Based on the generally upward flow of fluid within an ESP, sand could settle to the inlet of the interstage seals and produce significantly higher local sand concentrations. Seals tested at a high sand concentration show some three-body abrasion at the inlet, but this did not

meaningfully impact the wear rate. Future work should relate sand concentration at the inlet of an ESP to sand concentration passing through interstage seals.

The presence of gas modestly increases wear rate. Stains from heat checking are observed on reinforced thermoplastics operated with high GVFs. The presence of gas created low frequency vibrations, which produced large vibration orbit variability at large clearances.

Axial grooves are ineffective at preventing wear for the sand concentrations tested. Reinforced thermoplastic seals wore from three-body abrasion at the same rate regardless if the seal was plain or grooved. Carbide seals primarily wore from sliding wear, which was not affected by the presence of axial grooves. Axial grooves significantly increased leakage, which would decrease pump performance.

Results indicate plain self-mated carbide seals should be used in ESPs. Differences between SiC and WC are minimal, suggesting either material would be suitable for use in ESPs. Fracture failure remains a significant concern for carbide seals. Future work should focus on protecting carbide seals from blunt forces. Additional work could also focus on developing programs to project interstage seal wear and ESP lifetimes.

REFERENCES

[1] Breit, Steve, and Ferrier, Neil. “Using ESPs for artificial lift.” *Pumps & Systems.* Web. (2011).

[2] Rivera, R., Director, Kinetic Pump Innovations, LP, Houston, TX, Personal Communication (2013).

[3] Childs, Dara W., Norrbin, Clay S., and Phillips, Stephen. “A Lateral Rotordynamics Primer on Electric Submersible Pumps (ESPs) for Deep Subsea Applications.” *Proceedings of the 43rd Turbomachinery & 30th Pump Users Symposia.* Houston, TX, September 23-25, 2014. DOI: https://doi.org/10.21423/R15K8Q

[4] Morrison, Gerald L., Saleh, Ramy, Carvajal, Nicolas, and Bai, Changrui. “The Measured Impact of Erosion on the Rotodynamic and Performance Characteristics of a Mixed Flow ESP.” *Proceedings of the 44th Turbomachinery & 31st Pump Users Symposia.* Houston, TX, September 14-17, 2015. DOI: https://doi.org/10.21423/R17W6P

[5] von Flatern, Rick. "Electrical Submersible Pumps." *Oilfield Review* (2015).

[6] Scarsdale, Kevin. “ESP Qualification and Reliability.” *Multiphase Pump User Roundtable (MPUR).* Houston, TX, 2012.

[7] Durham, Marcus O., Williams, James H., and Goldman, Dwight J. “Effect of Vibration on Electric Submersible Pump Failures.” *SPE Journal of Petroleum Technology*. Vol. 42 No 2 (1990): pp. 186-190. DOI: https://doi.org/10.2118/16924-PA

[8] Lomakin, A. “Calculation of Critical Number of Revolutions and the Conditions Necessary for Dynamic Stability of Rotors in High-Pressure Hydraulic Machines when Taking into Account Forces Originating in Sealings.” *Power and Mechanical Engineering*, April (1958).

[9] Iwatsubo, T., and Nishino, T. “An Experimental Study on the Static and Dynamic Characteristics of Pump Annular Seals.” *Seventh Workshop on Rotordynamic Instability Problems in High Performance Turbomachinery*. College Station, TX. May 10–12, 1993. pp. 30–45. DOI: https://doi.org/10.1299/kikaic.55.310

[10] Forsberg, M. “Evaluation of ESP Vibration: Technical Process versus Black Magic.” *Society of Petroleum Engineers ESP Workshop*. Houston, TX, 2013.

[11] Dufrane, K. F., Kannel, J. W., and McCloskey, T. H. "Wear of Steam Turbine Journal Bearings at Low Operating Speeds." *J. of Lubrication Tech* Vol. 105 No. 3 (1983): pp. 313-317. DOI: 10.1115/1.3254599

[12] Szeri, Andras Z. *Fluid Film Lubrication, 2nd Ed*. Cambridge University Press, New York (2011).

[13] Ju, Frederick D., and Huang, John H. “Heat checking in the contact zone of a bearing seal (a two-dimensional model of a single moving asperity).” *Journal of Wear*, Vol. 79 No. 1 (1982): pp. 107-118. DOI: https://doi.org/10.1016/0043-1648(82)90207-1

[14] Xuan, J.L., Hong, I.T., and Fitch, E. C. “Hardness Effect on Three-Body Abrasive Wear Under Fluid Film Lubrication”. *ASME J. Tribol.* Vol. 111 No. 1 (1989): pp. 35-40. DOI: 10.1115/1.3261876

[15] Archard, J. F. “Wear Theory and Mechanisms.” *Wear Control Handbook*, Peterson, M. B. and Winer, W. O., (eds), ASME, New York, 1980, pp 35-80.

[16] Takacs, Gabor. *Electrical Submersible Pump Manual: Design, Operations, and Maintenance*. Gulf Professional Publishing, Burlington (2009).

[17] Carvajal Diaz, Nicolas I. “Effects of sand on the components and performance of electric submersible pumps”, M. S. Thesis, Texas A&M University, College Station, TX. 2012.

[18] Saleh, Ramy. “Experimental testing of an electrical submersible pump undergoing abrasive slurry erosion”, M. S. Thesis, Texas A&M University, College Station, TX. 2013.

[19] Zheng, Dhezi. “Three-Phase Erosion Testing and Vibration Analysis of an Electrical Submersible Pump”, M. S. Thesis, Texas A&M University, College Station, TX. 2013.

[20] Bai, Changrui. “Rotordynamic and Erosion Study of Bearings in Electrical Submersible Pumps”, Ph. D. Dissertation, Texas A&M University, College Station, TX. 2017.

[21] Steck, Daniel D’Andrea. “Experimental study of multiphase pump wear”, M. S. Thesis, Texas A&M University, College Station, TX. 2014.

[22] Chen, Yi. “Three phase erosion testing and CFD analysis of a helicon axial pump”, Ph.D. Dissertation, Texas A&M University, College Station, TX. 2017.

[23] Johnson, Andrew William. “Development and validation of an electric submersible pump bearing erosion facility that replicates the conditions experienced during pump operation”, M. S. Thesis, Texas A&M University, College Station, TX. 2015.

[24] Ying, T. N., Shen, M. C., Wang, Y. S., and Hsu, S. M. “Tribology of Si-Based Ceramics: Wear Mechanisms”. *Tribology Transactions.* Vol. 40 No. 4 (1997): pp. 685-693. DOI: https://doi.org/10.1080/10402009708983709

[25] Lu, Dun, Liu, Kejia, Zhao, Wanhua, and Lu, Bingheng. “Thermal Characteristics of Water-Lubricated Ceramic Hydrostatic Hydrodynamic Hybrid Bearings”. *Tribology Letters.* Vol. 63 No. 23 (2016): pp. 1-10. DOI: https://doi.org/10.1007/s11249-016-0711-x

[26] Andersson, Peter. “Water-Lubricated Pin-on-Disc Tests with Ceramics.” *Wear.* Vol. 154 No. 1 (1992): pp. 37-47. DOI: https://doi.org/10.1016/0043-1648(92)90241-Y

[27] “Durable Tungsten Carbide for Extreme Service Applications.” *Coorstek.* Web. (2017).

[28] Wakigawa, Asahiro, Aiyoshizawa, Shunichi, Takagi, Kiyokazu, and Konno, Daisuke. “A Study of Ceramic Bearing for Vertical Pumps (Wear of a Submersible Bearing in Slurry).” *JSME Intl.* Vol. 31 No. 2 (1988): pp. 263-268. DOI: https://doi.org/10.1299/jsmeb1988.31.2_263

[29] “Tungsten Carbide – An Overview.” *AZO Materials*. Web (2018).

[30] “Polyketones (PEEK, PEKK).” *Vertec*. Web. (2007).

[31] Yao, Shan-Shan, Jin, Fan-Long, Rhee, Kyong Yop, Hui, David, and Park, Soo-Jin. “Recent advances in carbon-fiber-reinforced thermoplastic composites: A review”. *Composites Part B.* Vol. 142 No. 1 (2018): pp. 241-250. DOI: https://doi.org/10.1016/j.compositesb.2017.12.007

[32] Yamamoto, Y., and Takashima, T. “Friction and wear of water lubricated PEEK and PPS sliding contacts.” *Wear* Vol. 253 No. 7-8 (2002): pp. 820-826. DOI: https://doi.org/10.1016/S0043-1648(02)00059-5

[33] Clarke, C. G., and Allen C. “The water lubricated, sliding wear behaviour of polymeric materials against steel.” *Tribol Int* Vol. 24 No. 2 (1991): pp.109-118. DOI: https://doi.org/10.1016/0301-679X(91)90041-7

[34] Hanchi, J, and Eiss, NS. “Dry sliding friction and wear of short carbon-fiber-reinforced polyetheretherketone (PEEK) at elevated temperatures.” *Journal of Wear* Vol. 203-204 (1997): pp. 380–386. DOI: https://doi.org/10.1016/S0043-1648(96)07347-4

[35] Xie, G. Y., Sui, G. X., and Yang, R. “Effects of potassium titanate whiskers and carbon fibers on the wear behavior of polyetheretherketone composite under water lubricated condition.” *Composites Science and Technology* Vol. 71 No. 6 (2011): pp. 828-835. DOI: https://doi.org/10.1016/j.compscitech.2011.01.019

[36] Swierczek, Martin. “Using Thermoplastic Composite Bearings in Vertical Water Pumps.” *Pumps & Systems.* Web. (2014).

[37] San Andrés, Luis, and Lu, Xueliang. “Leakage, Drag Power and Rotordynamic Force Coefficients of an Air in Oil (Wet) Annular Seal.” *J. Eng. Gas Turbines Power*. Vol. 140 No. 1 (2017): pp. 1-11. DOI: 10.1115/1.4037622

[38] Brennen, Christopher Earls. “Radial and Rotordynamic Forces.” *Hydrodynamics of Pumps*. Cambridge University Press, New York (1994): pp. 209-252.

[39] Childs, Dara. “Dynamic Analysis of Turbulent Annular Seals Based On Hirs’ Lubrication Equation.” *J. Eng. Lubrication Tech*. Vol. 105 No. 3 (1983): pp. 429-436. DOI: 10.1115/1.3254633

[40] Childs, Dara. “Rotordynamic Models for Liquid Annular Seals.” *Turbomachinery Rotordynamics: Phenomena, Modeling & Analysis*. John Wiley and Sons, New York (1993): pp. 227-289.

APPENDIX

XLTRC2 SEAL MODELING

Seal geometries and test conditions modeled in XLTRC2 using the programs "Hseal_mix[7]" and "XLHsealH[8]" provide a better understanding of experimental data by estimating displacements and forces. Seals without axial grooves are studied based on program capabilities. Unless otherwise stated, simulations utilize conditions identical to experimental tests. Seal and shaft material properties do not affect these predictions, as only geometry and test conditions contribute to seal reaction forces. For all simulations, XLTRC2 programs predicted inertial coefficients of zero, denoting no added mass. Reynolds numbers transitioned from below $2x10^3$ for clearances below 127 μm (laminar flow) to $1.2x10^4$ for clearances above 508 μm (turbulent flow).

The impact of inlet swirl ratio[9] was investigated, which can significantly affect force coefficients for short seals. Figure A-1 shows the effect of typical inlet swirl ratios is negligible for the shorter length carbide seal, indicating swirl brakes would have minimal impact for the given operating conditions. An inlet swirl ratio of 0.4 is chosen for simulations based on the study performed by Childs et al. [3].

---

[7] Copyright 2017 by Texas A&M University Turbomachinery Laboratory. All rights reserved. Dr. Luis San Andrés and Xueliang Lu

[8] Copyright 2010 by Texas A&M University. All rights reserved. Dr. Luis San Andrés

[9] Inlet swirl ratio is the ratio of tangential fluid velocity to tangential rotor velocity

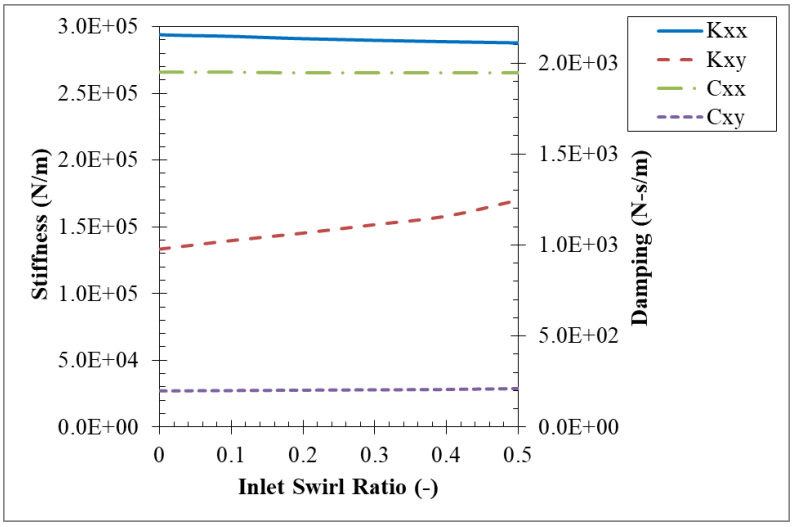

Figure A- 1 Force coefficients as a function of inlet swirl ratio for a carbide seal with 127 µm of radial clearance

Figure A-2 shows direct stiffness as a function of radial clearance for test conditions at 0% GVF and zero eccentricity. The 50% greater length of the thermoplastic seal largely accounts for differences in force coefficients between the thermoplastic and carbide seal. Figure A-2 shows stiffness peaks around 125 µm radial clearance; a local minima in direct stiffness occurs around 175 µm as flow transitions from laminar to turbulent. Beyond 200 µm, stiffness steadily decays. Figures A-3 & A-4 show direct and cross-coupled stiffness and damping for both seals.

In Fig. A-2, the carbide seal calculated direct stiffness is negative at zero eccentricity for radial clearances below 50 µm. Negative direct stiffness indicates the fluid film provides no direct support for the shaft, which would cause the shaft to deflect until the fluid film provides adequate stiffness. This is expected for tight clearances that circumvent the Lomakin effect, as explained by Brennen [38] from analysis by Childs [39]. This behavior can also be explained by the fact that cavitation is not predicted unless the rotor has a large eccentricity, preventing the generation of hydrodynamic stiffness.

Figure A-5 shows no inlet pressure drop is created for clearances that generate negative direct stiffness; the pressure differential across the seal is entirely absorbed by friction flow losses through the seal, preventing the creation of direct stiffness through the Lomakin effect. Friction losses account for less of the pressure differential at larger clearances, allowing the generation of stiffness through the Lomakin effect.

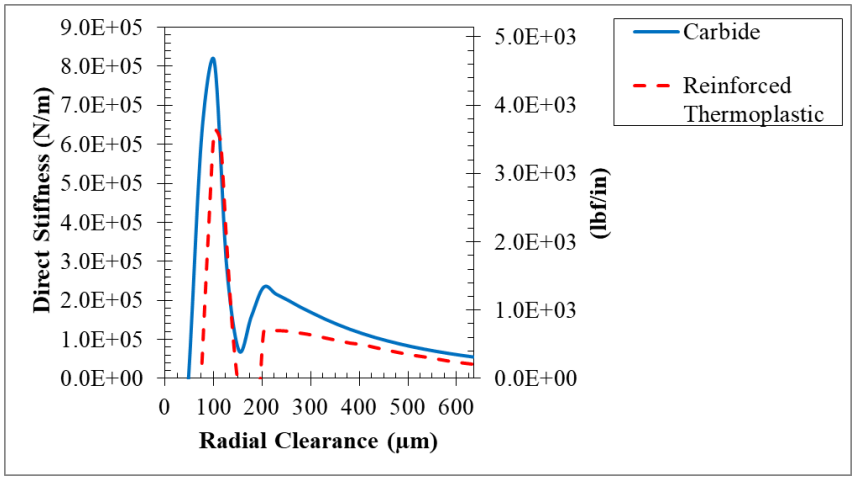

Figure A- 2 Direct stiffness as a function of radial clearance at test conditions and 0% GVF at zero eccentricity

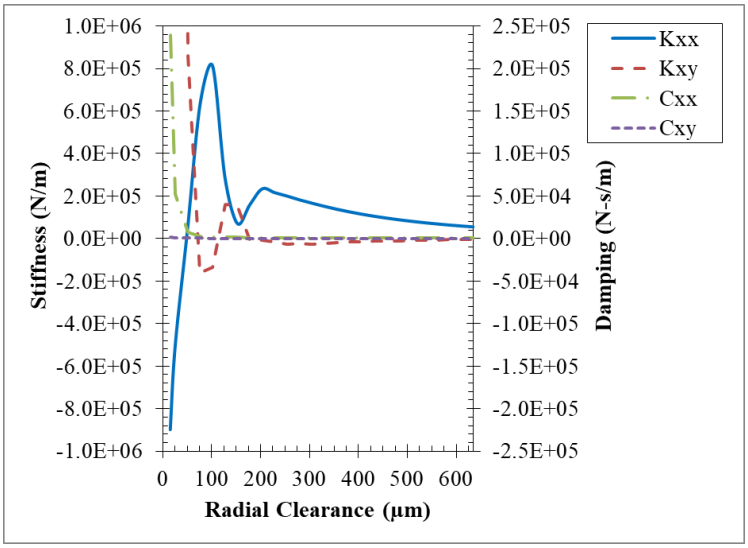

Figure A- 3 Simulated force coefficients for carbide seals at test conditions and 0% GVF at zero eccentricity

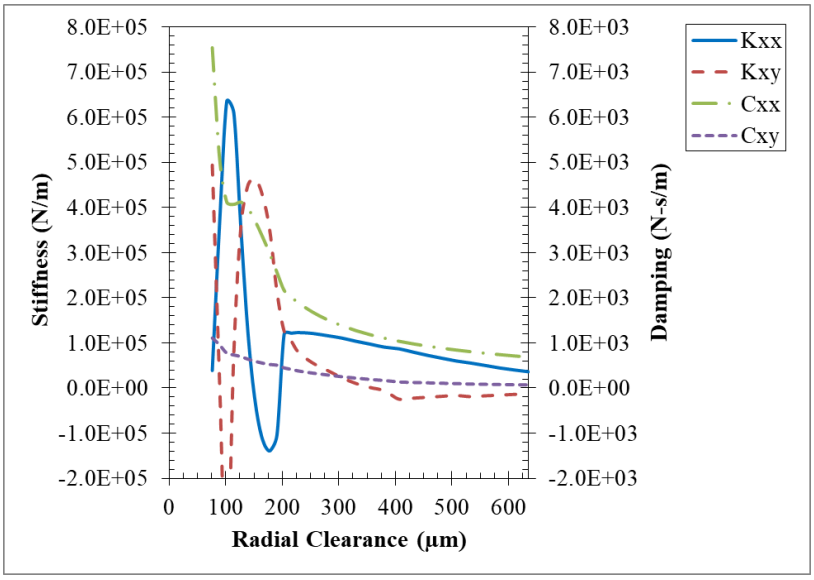

Figure A- 4 Simulated force coefficients for reinforced thermoplastic seals at test conditions and 0% GVF at zero eccentricity

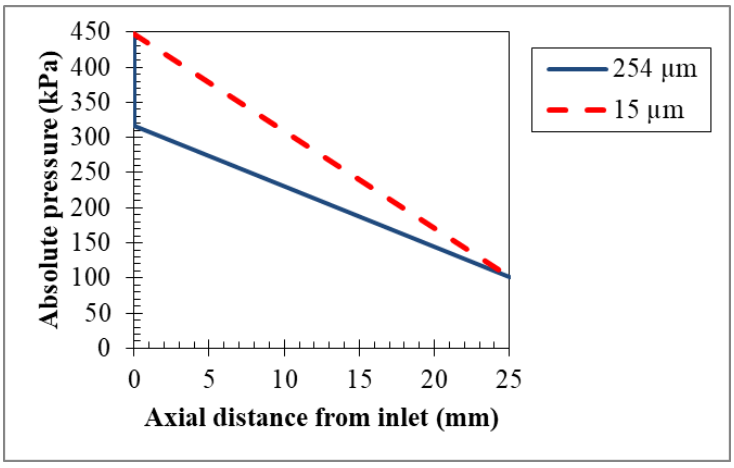

Figure A- 5 Simulated pressure profile at different initial radial clearances of carbide seals for test conditions and 0% GVF at zero eccentricity

According to Childs [40], force coefficients are generally constant for eccentricities less than 0.5. Figures A-6 & A-7 show force coefficients as a function of eccentricity for the test seals, and Figs. A-8 & A-9 show radial reaction force as a function of eccentricity or film thickness for different clearances. Force coefficients are roughly constant for eccentricities less than 0.8 and clearances greater than 50 µm, denoted by a linear relationship between radial force

and eccentricity. Radial force is a function of film thickness rather than eccentricity for film thicknesses less than 25 µm, when partial or boundary lubrication would occur with asperity contact. Cavitation is predicted for non-centered shafts when minimum film thicknesses are less than 25 µm. Figure A-10 shows tangential force generated from shaft deflections increases with increased eccentricity and decreased clearance. Tangential force is consistently positive, denoting a tendency to precess in the direction of shaft rotation.

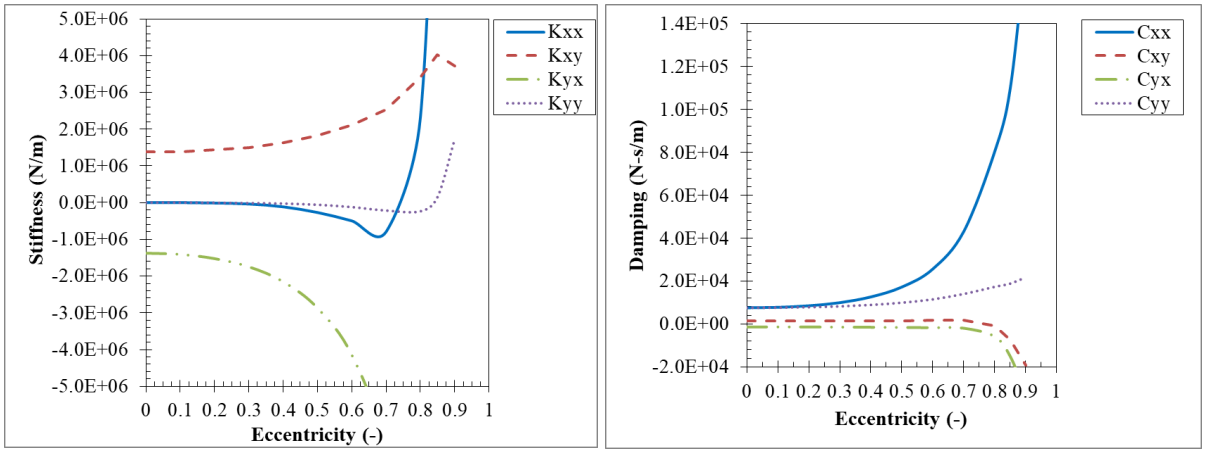

Figure A- 6 Stiffness and damping coefficients as eccentricity in the x direction is varied for reinforced thermoplastic seals with 76 µm of radial clearance, 0% GVF and test conditions.

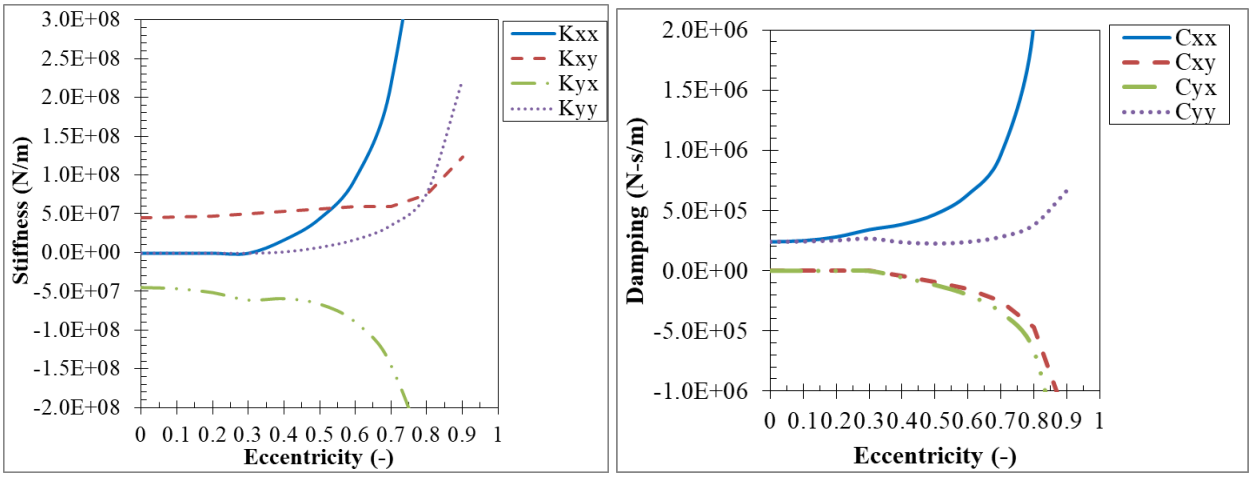

Figure A- 7 Stiffness and damping coefficients as eccentricity in the x direction is varied for carbide seals with 15 µm of radial clearance, 0% GVF and test conditions

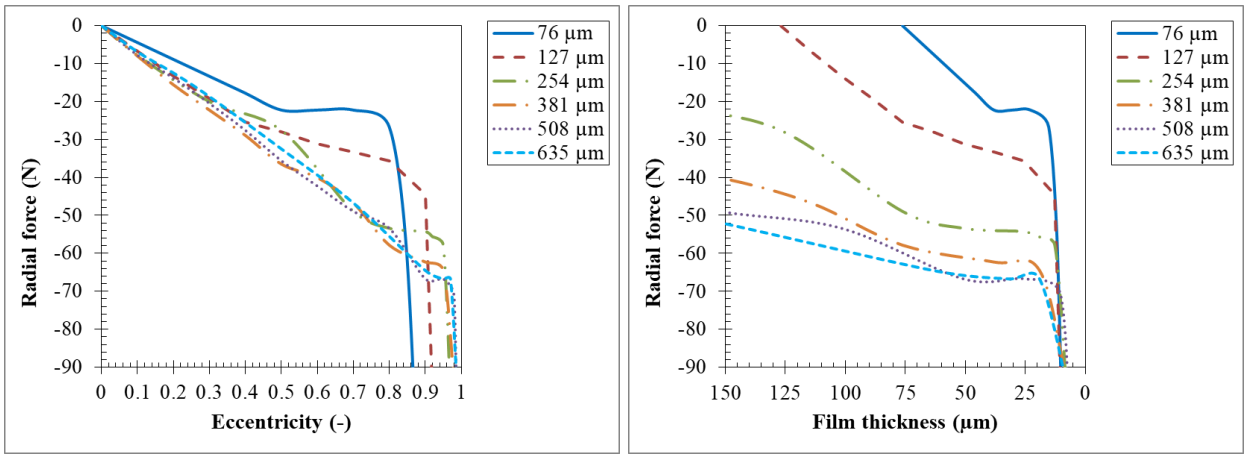

Figure A- 8 Radial force as a function of eccentricity and film thickness for reinforced thermoplastic seals with different radial clearances, 0 % GVF and test conditions

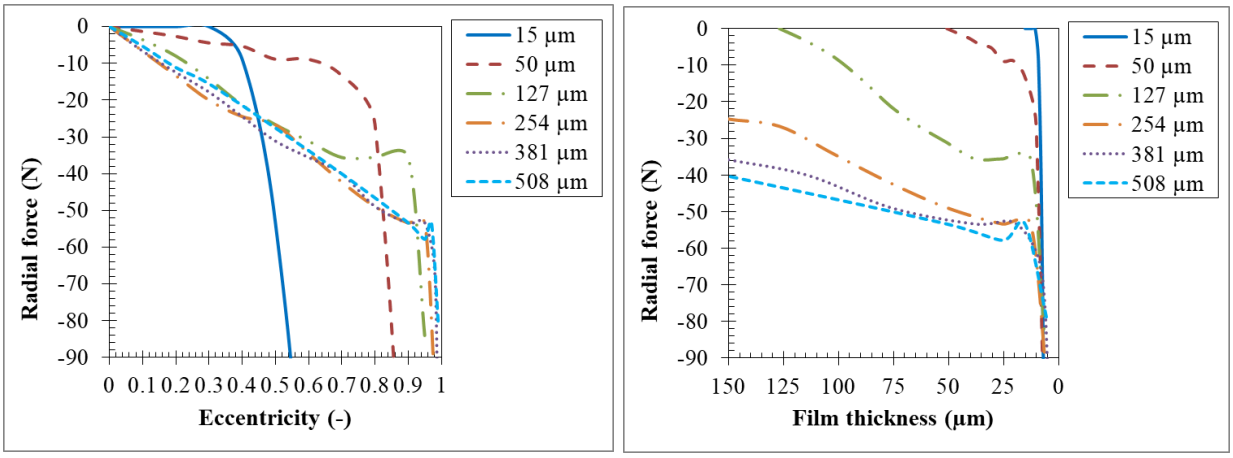

Figure A- 9 Radial force as a function of eccentricity and film thickness for the carbide seal with different radial clearances, 0 % GVF and test conditions

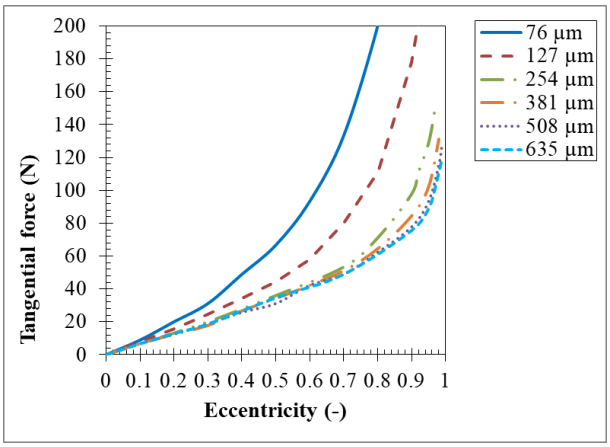

a) reinforced thermoplastic

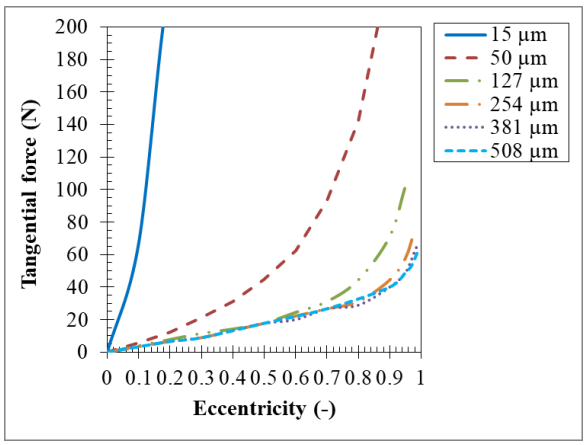

b) carbide

Figure A- 10 Tangential force as a function of eccentricity for the reinforced thermoplastic and carbide seals with different radial clearances, 0 % GVF and test conditions

Forces and moments from lateral and angular displacements may be significant for *L/D* ratios above 0.75 [40]. While the carbide seal has an *L/D* of 0.59, the reinforced thermoplastic seal has an *L/D* of 0.80. For film thicknesses greater than 25 µm, simulations of the reinforced thermoplastic seal predicted negligible forces from angular deflections and negligible moments.

The impact of gas volume fraction (GVF) on seal rotordynamics is also studied. Pressure generally decreases with axial position within seals, causing GVF to increase as gases expand. An inlet GVF of 20% produces an outlet GVF of 53%, while an inlet GVF of 80% produces and outlet GVF of 95%. Adding air greatly reduces the speed of sound from 1,400 m/s at 0% GVF to 24 m/s at 20% GVF, generating mach numbers as high as 0.90. Figures A-11 & A-12 show the presence of air significantly decreases the radial and tangential forces supplied by the seal.

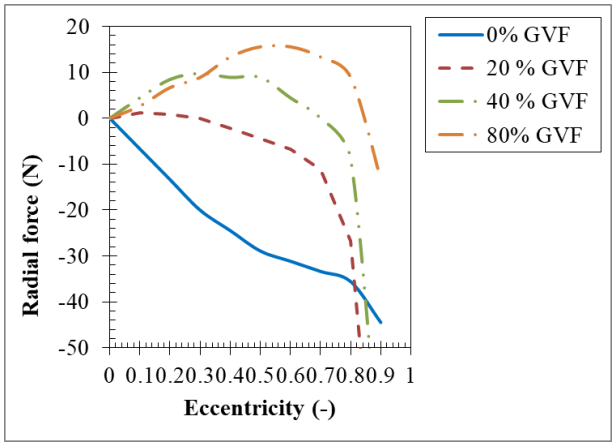

a) 127 µm

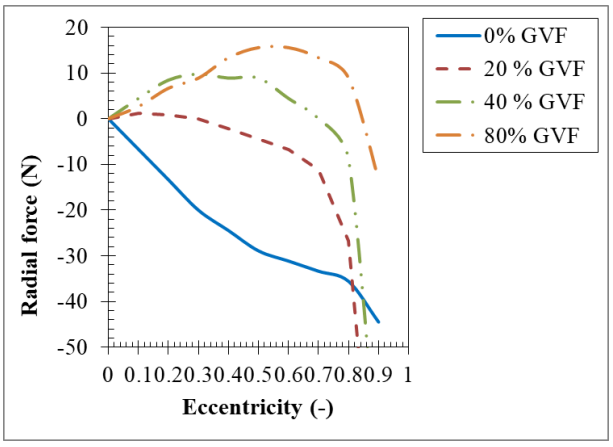

b) 381 µm

Figure A- 11 Radial force as a function of eccentricity for the reinforced thermoplastic seal at different GVFs and test conditions

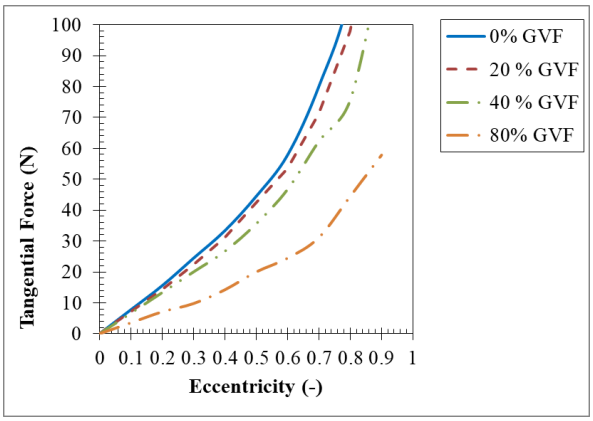

a) 127 µm

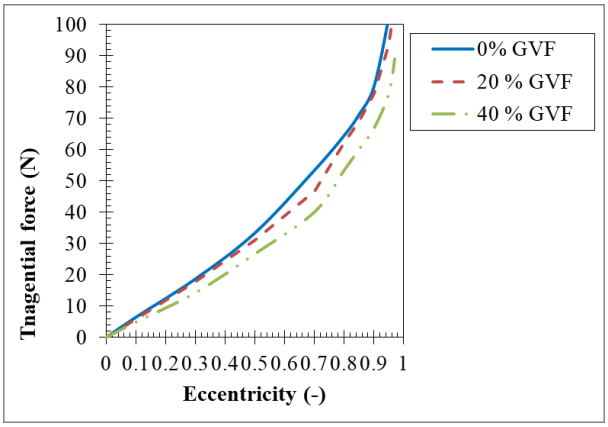

b) 381 µm

Figure A- 12 Tangential force as a function of eccentricity for the reinforced thermoplastic seal at different GVFs and test conditions